

Fermi National Accelerator Laboratory

FERMILAB-Conf-98/398

The Physics of Jets

Hugh E. Montgomery

*Fermi National Accelerator Laboratory
P.O. Box 500, Batavia, Illinois 60510*

January 1999

Published Proceedings of *Oeme Ecole d'Ete de Physique des Particules (Ecole de Gif-sur-Yvette)*,
CentCPPM, Marseille, France, September 7-11, 1998

Operated by Universities Research Association Inc. under Contract No. DE-AC02-76CH03000 with the United States Department of Energy

Disclaimer

This report was prepared as an account of work sponsored by an agency of the United States Government. Neither the United States Government nor any agency thereof, nor any of their employees, makes any warranty, expressed or implied, or assumes any legal liability or responsibility for the accuracy, completeness, or usefulness of any information, apparatus, product, or process disclosed, or represents that its use would not infringe privately owned rights. Reference herein to any specific commercial product, process, or service by trade name, trademark, manufacturer, or otherwise, does not necessarily constitute or imply its endorsement, recommendation, or favoring by the United States Government or any agency thereof. The views and opinions of authors expressed herein do not necessarily state or reflect those of the United States Government or any agency thereof.

Distribution

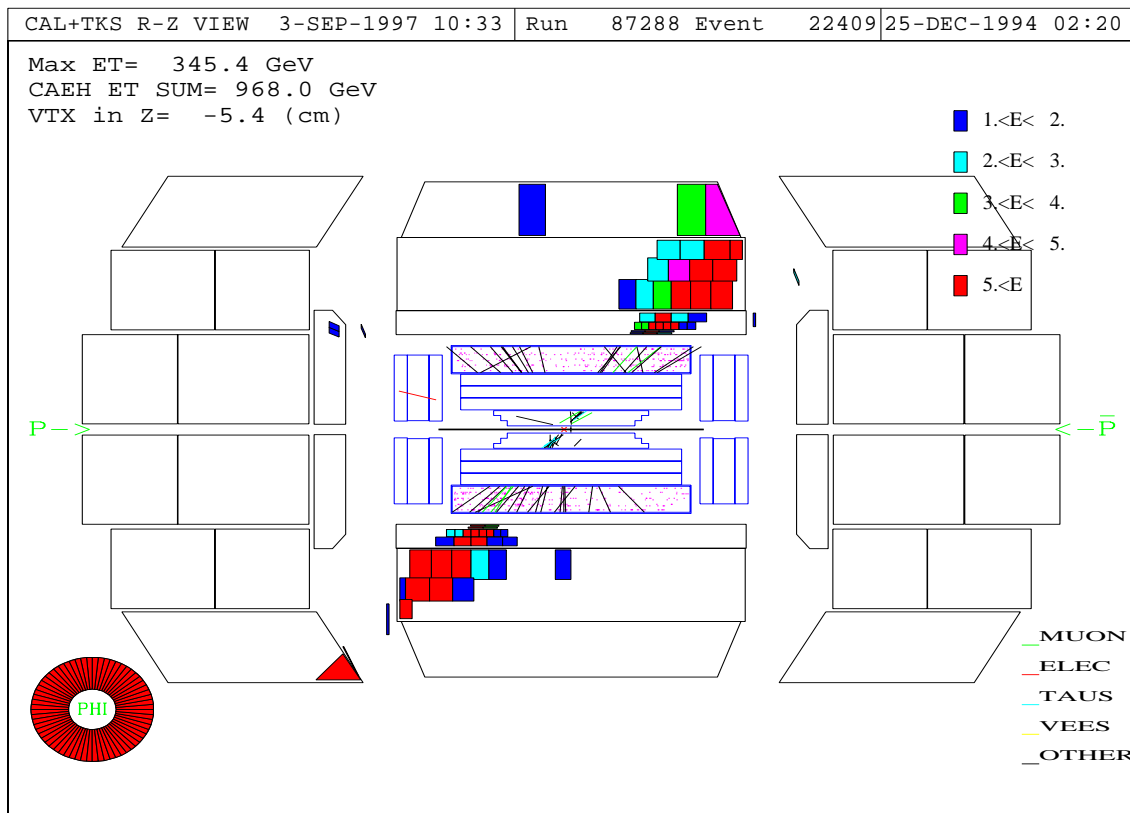
Approved for public release; further dissemination unlimited.

Copyright Notification

This manuscript has been authored by Universities Research Association, Inc. under contract No. DE-AC02-76CHO3000 with the U.S. Department of Energy. The United States Government and the publisher, by accepting the article for publication, acknowledges that the United States Government retains a nonexclusive, paid-up, irrevocable, worldwide license to publish or reproduce the published form of this manuscript, or allow others to do so, for United States Government Purposes.

The Physics of Jets

Hugh E. Montgomery
Fermi National Accelerator Laboratory
P.O. Box 500
Batavia, IL60510 U.S.A.



Abstract

Jets are important objects in particle physics. Their accurate measurement enables a large fraction of the current and future physics at hadron colliders. In these lectures we discuss jets, how they are measured, how those measurements are calibrated and some of the physics that can be done with them.

Contents

1	Introduction	3
2	Partons to Jets	4
3	Jet Calibration	6
3.1	Jet Response and Resolution: CDF	7
3.2	Jet Calibration: $D\bar{O}$	9
3.2.1	Jet Resolution	9
3.2.2	Energy Calibration	10
4	Physics with Single Jets	12
5	Physics with Multi-Jet Systems	15
5.1	Compositeness	15
5.2	Dijet Cross Sections	15
5.3	Dijet Angular Distributions	16
5.4	Dijet Masses	17
5.5	Higher Jet Multiplicities	17
5.6	Diffractional Jets	19
6	The Drell-Yan Process	21
7	Jets with Electroweak Bosons	22
7.1	Vector Boson Transverse Momenta	22
7.2	Vector Bosons and Jets	23
8	Jet Spectroscopy	24
8.1	$W \rightarrow jets$	25
8.2	$Z \rightarrow jets$	26
8.3	Higher mass boson searches	26
8.4	Jet Spectroscopy in Top Decays	27
8.5	Higgs $\rightarrow jets$	32
9	Summary	32
10	Acknowledgements	32

1 Introduction

When we discuss high energy physics processes[1] the quarks are treated as fundamental constituent objects of the theory and gluons are treated as fundamental gauge bosons. However, each of these objects is colored, in the quantum chromodynamic sense, and so, in general, does not survive long enough for them to be directly detected. Instead these partons are dressed by soft QCD processes into observable hadrons, usually many of them. The hadrons appear in the detector as jets, clusters of energy in the calorimeter. A rather striking example is illustrated on the cover where a side view of the DØ detector is shown. A similar event from a different view in the CDF detector is shown in Fig. 1.

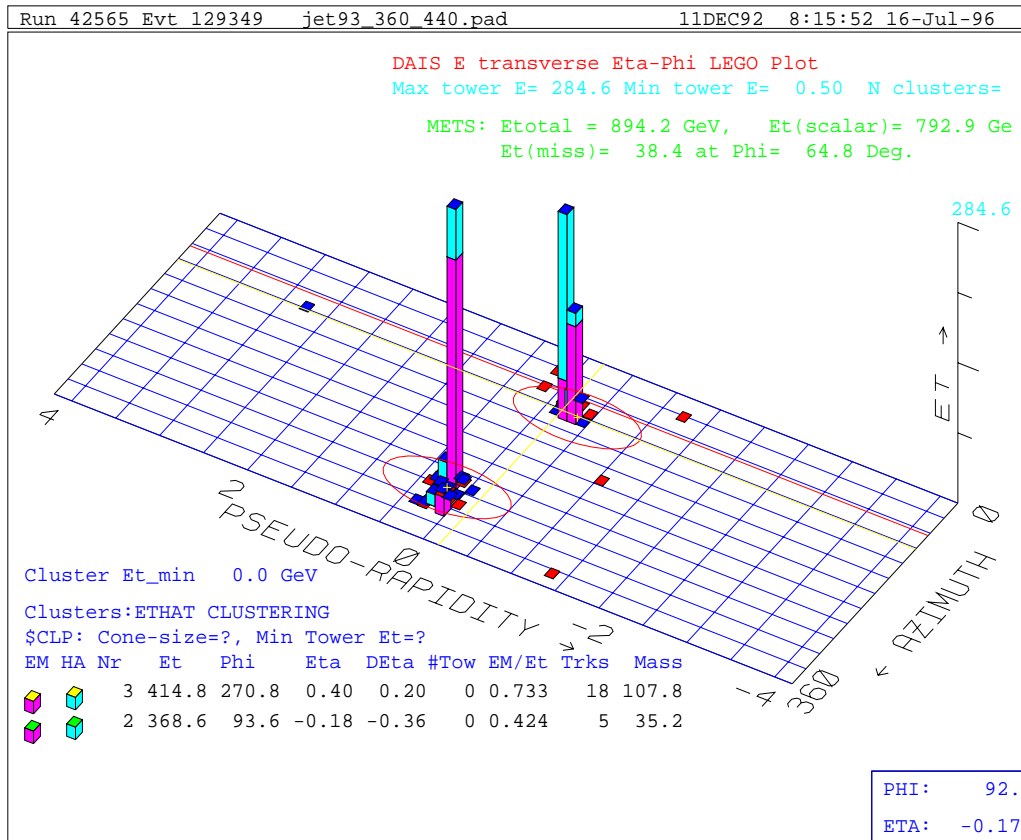


Figure 1: An example of a $p\bar{p}$ interaction in which two jets are observed in the CDF detector. In this case the transverse energy deposited in the calorimeter cells is shown. The height of the column in each cell is proportional to the transverse energy in that cell.

In these two events we can see that the concept of a jet is directly motivated by what is observed in the detector. However, these are two rather clean events at very high transverse energy, E_T . At lower energies and in more complex events, care is needed in the construction of jets. Furthermore, quantitative comparisons with theory demand that the jets, their definition and their calibration, be approached systematically.

In these lectures we do not attempt a review[2] of all the relevant physics results from jets, rather we try and give some sense of the methodology. In section 2 we give a little

theoretical foundation; however, this is primarily to get us started and we shall try to take a data driven approach. In section 3 we discuss the calibration of the observed jets and in section 4 we discuss the inclusive jet spectrum, the simplest of all measurements, and its comparison with the QCD predictions. In section 5, we discuss multi-jet final states, first of all with two jets observed corresponding to the simplest parton scattering, then with as many as six final state jets. In QCD terms rather high order calculations, albeit the simplest aspects, are used to describe the data and remarkable success is enjoyed.

The dijet systems provide a sensitivity to possible compositeness of the constituents we currently consider to be fundamental. To complete this discussion of compositeness, we take a diversion from jets in section 6, and discuss dilepton production and the Drell-Yan process. The simplest mechanism for heavy vector boson production is the Drell-Yan diagram, however at high energies we can supplement these studies by looking at the transverse momenta of vector bosons and the associated jets; this is discussed in section 7.

In section 8 we start to take the concept that we have reconstructed the final state partons in the event more seriously. We attempt to combine the parton jets and to identify the effective masses of these systems with objects which have or could have decayed into these partons. In particular we examine the hadronic decays of vector bosons and the search for their siblings at higher masses. We examine the multijet $t\bar{t}$ systems; here the reconstruction of multijet decays has led to the determination of the mass of the top quark. The precision achieved is directly related to the precision with which we are able to calibrate the parton jet energies. Briefly we look ahead to the search for the Higgs boson through its decays to jets in order to set the table for the next few years of experimentation. In section 9 we summarise.

We will use primarily the publications and techniques of the CDF and DØ experiments operating at the Tevatron $\bar{p}p$ Collider to illustrate the discussion.

2 Partons to Jets

The kinematics of particles in hadron colliders is nicely treated by Baden[3]; he also covers the combination of energy depositions into jets. We can see from the event illustrated on the cover of this article and that shown in Fig. 1 that it is easy to justify and to define a jet as the energy deposited in a suitably defined region of the calorimeter.

From a theoretical point of view, we have been using the parton model and QCD as our paradigm since the early 1970's. In this model we envisage the nucleon as being composed of a number of point-like constituents, the quarks and gluons, collectively known as partons. The distribution of fractional momenta carried by each species of parton is described by a parton distribution function. These distributions are primarily determined by fitting a wealth of deep inelastic lepton scattering data[4].

The interaction between two nucleons is imagined to be the interaction between two partons in the initial state, with any other partons playing the role of spectators. The simplest interaction between the two partons is elastic and results in two partons in the final state. We can write the cross section for a generic hadron-hadron scattering process as the

convolution of the parton distribution functions with the hard parton-parton cross section,

$$\sigma \simeq \int \sum_{i,j} f_1^i(x_1, Q^2) \hat{\sigma}(x_1, x_2, Q^2) f_2^j(x_2, Q^2) dx_1 dx_2.$$

$f^{i,j}(x_{1,2}, Q^2)$ are the distribution functions of parton species i, j in terms of the momentum fractions $x_{1,2}$ of the proton carried by the partons. $\hat{\sigma}$ is the elementary parton-parton scattering cross section and Q^2 is the relevant hard scattering scale of the process.

We have never seen individual free partons. Rather, the partons fragment, emitting gluon radiation or splitting into quark-anti-quark pairs. This process is analogous to that in which an electron in matter generates an electromagnetic shower of electrons, positrons and photons. The emission angles are predominantly close to the direction of motion of the radiating partons and so the shower tends to be collimated. At some point the process stops with various of these many partons combining to form the colorless hadrons we actually observe. Empirically, all stages of this fragmentation process involve small angles such that the resulting hadrons have directions close to the parent parton. Hence a single final state parton results in a jet of observable particles.

We describe the kinematics of hadrons in hadron-hadron collisions using the transverse energy with respect to the collision axis E_T , and the pseudorapidity $\eta = -\ln \tan(\theta/2)$ where θ is the polar angle. For most applications the azimuthal angle(ϕ) is not a variable on which the physics depends. For massless, or very relativistic particles the pseudorapidity is a good approximation to the rapidity. Jets are reconstructed by summing the energy deposited in a defined region of (η, ϕ) space.

The most common approach is to define a circle in (η, ϕ) space and to position that circle such that it is centred on a cluster of cells with significant energy deposition. Such circles are indicated in Fig. 1. Imagining the particles emanating from an interaction vertex towards this circle we develop the picture of a cone and defining $\Delta R = \sqrt{\Delta\eta^2 + \Delta\phi^2}$ we call ΔR the ‘‘cone size’’. A typical cone size is $\Delta R = 0.7$ for many QCD studies, but in multi jet events, where the many cones could overlap, there are sometimes advantages to restricting the cone size to $\Delta R = 0.4, 0.5$ to enhance the reconstruction efficiency for the multiple jets. Practically we construct a vector sum of the cell energies. There are potentially many ways to proceed and some care has to be taken[5] that the definitions used in different experiments, and in the theory, are indeed equivalent.

The view that a jet which we have reconstructed contains all the particles from a primary final state parton is attractive but simplistic. We expect that sometimes the QCD fragmentation process will lead to a large angle emission of another parton. This parton may generate a distinct jet. At that point we can start to debate whether to, and how to, combine or associate jets. However, it is possible to study and test QCD by predefining a jet cone size and asking the theory to provide predictions with that same cone. We can make comparisons provided that we do the equivalent things with the data as with the theory. This is the attitude taken when we look at observables such as the distribution of transverse momenta of single jets. On the other hand, sometimes we really want to combine the observed jets so that we can ‘‘reconstruct’’ what we view as the primary partons. As we shall discuss later, this is the case when we try to use the jets we observe to determine the mass of their top-quark parent.

In e^+e^- and deep inelastic lepton scattering experiments, other jet reconstruction techniques are used. The k_T algorithm[6] has been proposed for use in $p\bar{p}$ interactions; it attempts to build jetlike entities from elementary energy objects (sometimes a combination of calorimeter and tracking information). In contrast to the cone algorithm, the k_T algorithm iteratively combines the elements using the relative transverse momentum as a resolution variable. Advocates of this approach argue that it is more consonant with the physical QCD process which leads to the observable hadrons and so has the potential to provide a better test of the theory and perhaps a better approach to parton reconstruction. Monte Carlo studies also suggest that the k_T algorithm is rather less sensitive to hadronisation effects. On the other hand the extent of the jet in the detector varies from jet to jet and this complicates the handling of instrumental and multiple interaction effects which deposit energy in the detector which is unrelated to the event under study. Nevertheless, as we heard in the questioning at the school, many are they who see the k_T algorithm as the wave of the future.

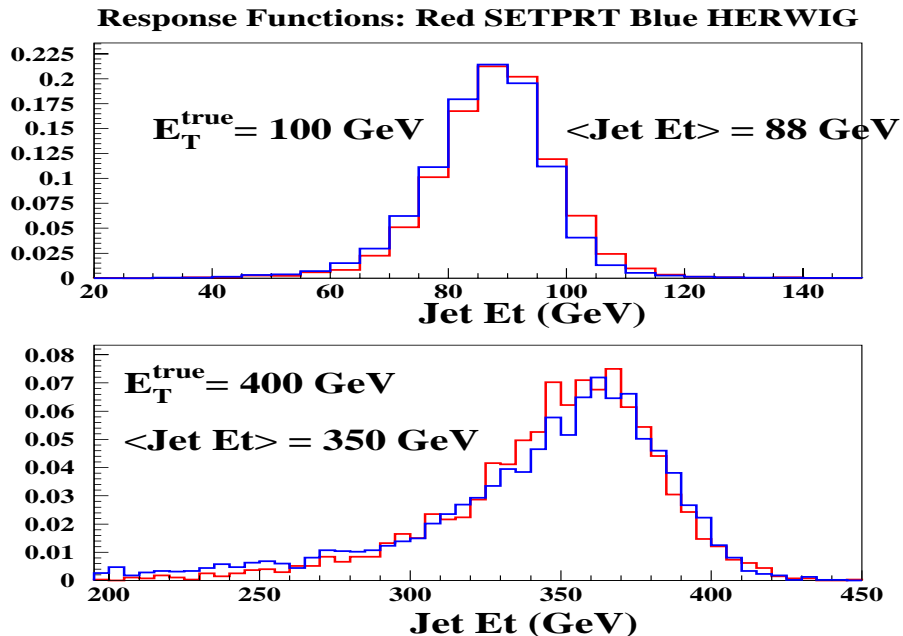


Figure 2: Jet energy response function for the CDF detector at 100 GeV and 400 GeV for two different simulations which are in good agreement.

3 Jet Calibration

The response of the calorimeter to individual particle types is in general different; the response to electrons of a given energy is higher than that to charged pions. There may also be non-linearities as a function of energy. There are cracks between cells and modules in the calorimeter construction. All these things, in conjunction with a variation from event to event of the composition and size of a jet as a result of the fragmentation process, make it

necessary to develop a detailed knowledge of the relationship between the observed and true energies of the jets.

The energy of a jet can be related to that observed with the expression

$$E = (E_{meas} - \mathcal{O}) / ((1 - \mathcal{S})R_{had}),$$

where \mathcal{S} is the correction to the observed energy in the cone due to the effects of energy leaking into or out of the cone during the showering process in the detector. It is to be emphasised that this is not a correction for the QCD “out-of-cone” radiation.

\mathcal{O} is the offset energy due to the sum of the instrumental noise, underlying event energy, and energy deposited by other interactions within the sensitive time of the calorimeter whether in the same bunch crossing or in preceding or subsequent crossings.

R_{had} is the energy response of the calorimeter to the jet.

In this section we discuss two different approaches to the determination of the calibration and to the related determination of the resolution.

3.1 Jet Response and Resolution: CDF

CDF measures the underlying event energy, the primary contribution to their offset \mathcal{O} , using minimum bias data. They find approximately 1 GeV for $\Delta R = 0.7$ cone jets. Those data were taken with a mean number of approximately 1.3 interactions per bunch crossing. CDF makes no attempt to apply a showering correction.

The CDF experiment bases its determination of the jet calibration[7] on extensive single particle measurements. The single particle measurements are made in a test beam where a wide range of particle energies is available and from *in situ* measurements of isolated single particles in the collider data, where the momenta are determined using the magnetic central tracking. These measurements yield response functions for single particle momenta down to 400 MeV.

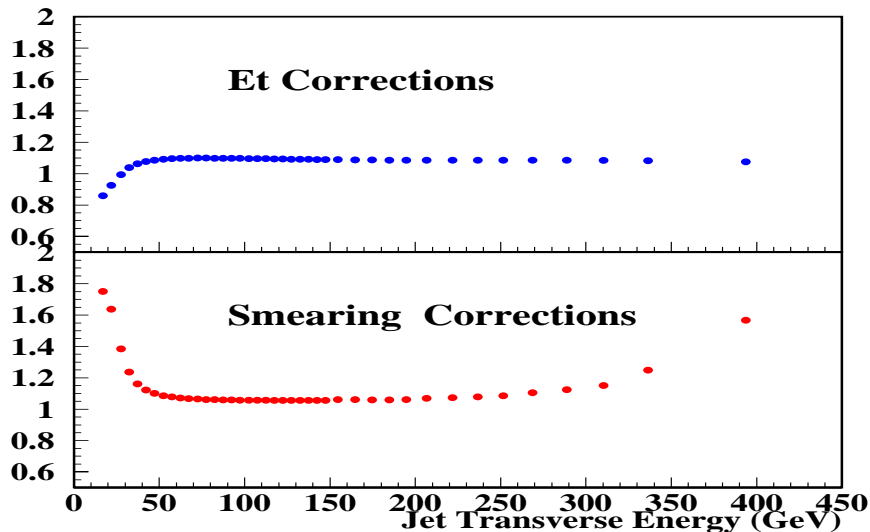


Figure 3: Jet energy and cross section corrections for CDF detector response to jets.

They construct both the effects of resolution and the calibration of the energy scale concurrently. The particles in jets are generated using both a Feynman-Field Monte Carlo and using Herwig. The Feynman-Field Monte Carlo was tuned to yield the observed multiplicity and momentum distribution of particles in jets in the data. The calibrated response is imposed particle by particle. As a result the response to a single jet is found. The distributions of that response to many jets is then the response function. Examples are shown in Fig. 2 for 100 GeV and for 400 GeV jets. The observed mean values are 88 GeV and 350 GeV, respectively. The difference between the two jet fragmentation models is very small. The width of the distribution is a representation of the resolution and they find $\sigma(E_T) \simeq 0.1E_T(\text{GeV}) + 1$ GeV for E_T between 35 GeV and 450 GeV. The tail to lower values in the 400 GeV reflects mainly the finite cracks between calorimeter cells.

In order to construct the corrections that need to be made for the single jet inclusive measurement, CDF uses a model for the cross section. They then convolute that cross section with the response functions described above. To obtain agreement with the uncorrected experimental data it is necessary to adjust the parameters of the model function. Once agreement is achieved, the mapping from a functional model to a smeared cross section provides them with the corrections which need to be applied to their data. Explicitly they construct two functions. The one in the top of Fig. 3 gives the correction to be made to the E_T scale. The second function shown in the bottom half of Fig. 3 gives the adjustment to the cross section at fixed transverse energy. We see that the E_T correction is rather constant except at very low transverse energies. The smearing correction is less than about 10% except at high and low transverse energies, where it can be quite large driven by the jet spectrum being steeper in those regions.

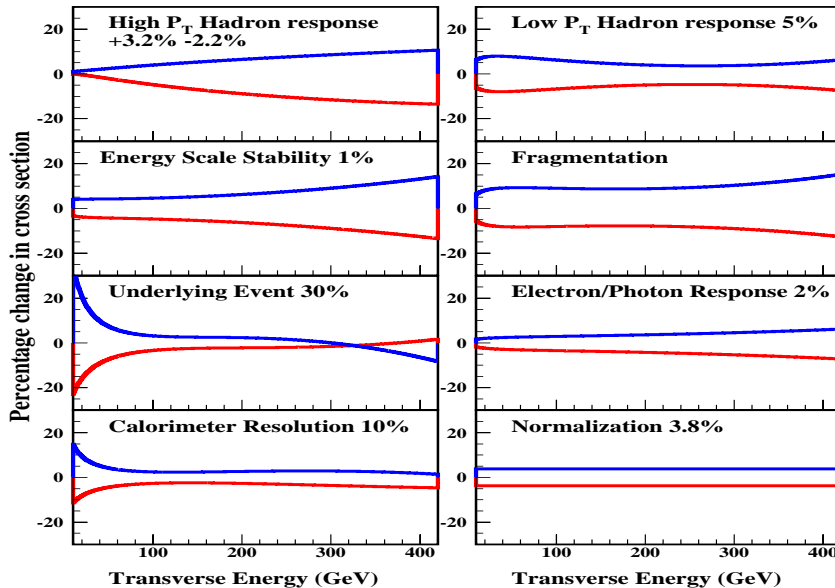


Figure 4: Components of the systematic errors in the determination of the uncertainty in the CDF measurement of the inclusive jet cross section due to the jet energy scale calibration.

In order to make the best use of their calibration work CDF considers the contributions of the various components to the uncertainties in the cross section, see Fig. 4, as a function of transverse energy. The eight uncertainties in the plot are derived by changing one component at a time in the MC simulation, such as low p_T hadron response, and then repeating the entire analysis. As a result, each of the uncertainties is independent of the other, and is 100% correlated from bin to bin in jet E_t .

For other analyses, CDF performs a correction jet by jet. Those corrections[8], which are not discussed here, also take into account the species of the jets.

3.2 Jet Calibration: DØ

The DØ experiment calibrates[9] its calorimeter jet response using collider data. The electromagnetic energy scale of the calorimeter is determined by the response to the electromagnetic decays of known particles, primarily the Z , but also the J/ψ and π^0 .

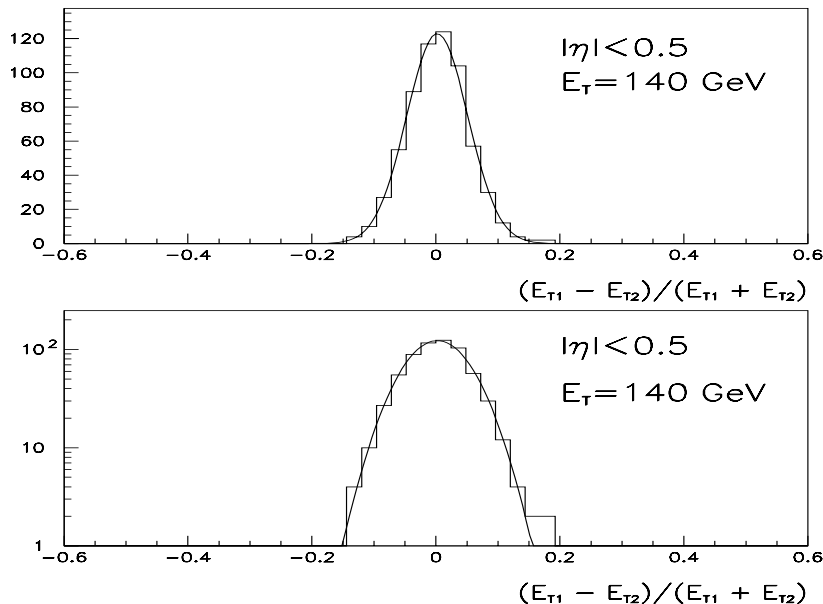


Figure 5: Transverse energy asymmetry between jets in two-jet events. E_{T1} and E_{T2} are the transverse energies of the two jets.

3.2.1 Jet Resolution

The jet energy resolution can be obtained from the distribution of relative response to jets in the limit that there are only two jets present in the events; for a perfect calorimeter the transverse energies in such an events should be equal. An asymmetry, the difference between the jet energies divided by their sum, is constructed. The distribution of this asymmetry for the DØ detector at 140 GeV is shown in Fig. 5 and we see that it is rather well described by a gaussian. This is a factor $\sqrt{2}$ times the resolution of a single jet. Similar distributions

allow the resolution to be determined as a function of transverse energy and DØ finds $\sigma(E_T) \sim 0.7\sqrt{E_T(\text{GeV})}$. Although the data samples are restricted to those cases where the jets are close to 180 degrees apart in azimuth there may still be undetected radiative jets below the reconstruction threshold. To correct for this the measurements are performed with upper limits of 20, 15, 12, 10 and 8 GeV on the transverse energy of possible accompanying radiated jets; they are then extrapolated to correspond to the limit of zero radiation.

The above discussion assumes no uncertainty in the vertex position. In the presence of vertex position errors in dijet events, the uncertainties in the transverse energies are correlated[10] and the simple asymmetry no longer reflects the calorimeter resolution. This is most pronounced when forward data are included in the sample. Nevertheless, by judicious choice of samples with different topologies the relevant energy resolutions can still be extracted from the data.

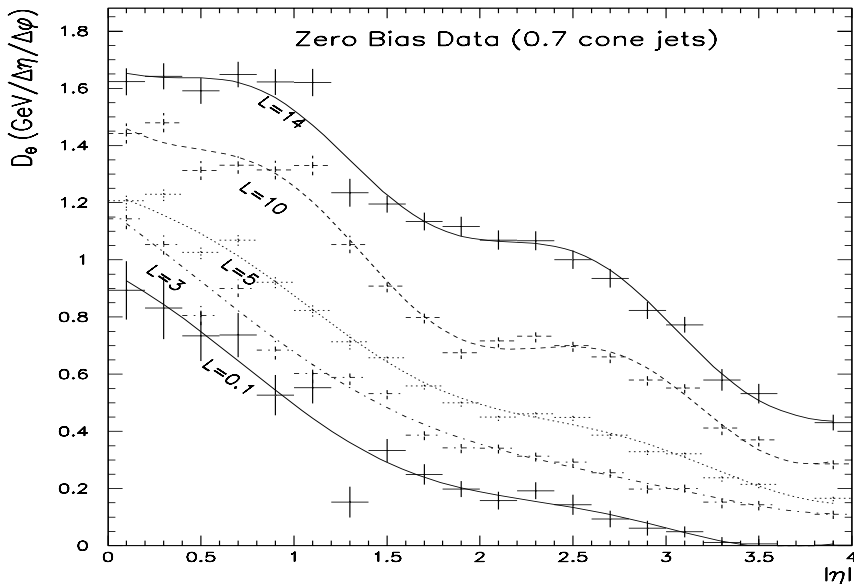


Figure 6: Transverse energy density in DØ measured using 0.7 cones and zero bias data.

3.2.2 Energy Calibration

DØ attempts to determine a showering correction \mathcal{S} . The determination is a little tricky; however, the correction is found to be essentially negligible for central jets with cone size 0.7. It can be substantial in the high η regions.

In the case of the DØ calorimeter the offset \mathcal{O} includes not only the underlying event but also the electronic noise and the energy deposited by the uranium decays. \mathcal{O} is determined by studying zero bias data. Zero bias data are taken during a store, in time with a bunch

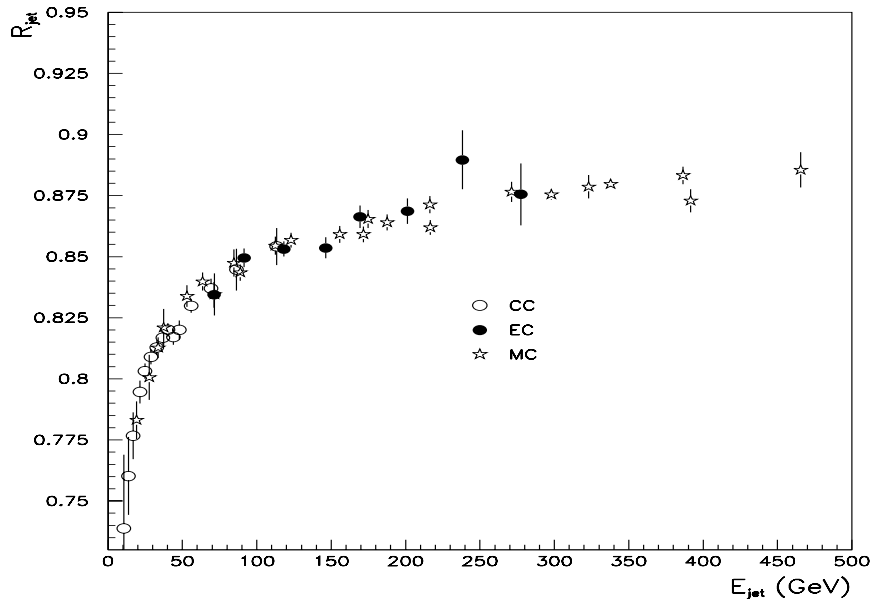


Figure 7: Jet energy response as a function of energy for jets in the DØ Central(CC) and End(EC) calorimeters and a comparison with Monte Carlo(MC).

crossing, but with no trigger requirement. Modulo subtleties associated with zero suppression in the readout, such a data set properly samples the offset energy. The result is going to be dependent on luminosity due to increased interaction probability and that is seen in Fig. 6 where we plot the transverse energy density as a function of pseudo-rapidity for different luminosities. Since the physical size of a 0.7 cone in the calorimeter reduces as the pseudo-rapidity increases, the offset further reduces when η increases. We can estimate from this plot that at zero luminosity the offset energy in a cone of size $\Delta R = 0.7$ is about 1 GeV. This is small and tractable for high energy jets but clearly for 20 GeV jets it is quite significant.

Having corrected the observed energy for the offset one determines the response using the missing energy (\cancel{E}_T) balance in events with a photon. A photon or a very electromagnetic jet has a response known from the electromagnetic calibration. In such events the \cancel{E}_T is expected to be zero except for calibration and resolution effects. By making a projection of the missing energy along the photon direction and demanding a balance, the calibration of the detector for jets is determined in a relatively algorithm independent manner. The relevant expression is

$$R_{had} = 1 + ((\cancel{E}_T \cdot \hat{n}^\gamma) / E_T^\gamma),$$

where \hat{n}^γ is the unit vector along the photon direction and E_T^γ is the photon transverse energy.

The measurement is limited by the relatively low $\gamma + jet$ rate to the region $E_T^\gamma \leq 150$ GeV. However DØ can use events with photons in the central calorimeter and jets in the end calorimeter. The end calorimeter uses the same technology as the central and, since for a given E_T the jet energy is higher, DØ can extend the method in energy. As a consequence R_{had} can be determined directly up to about 300 GeV as shown in Fig. 7. We also see that

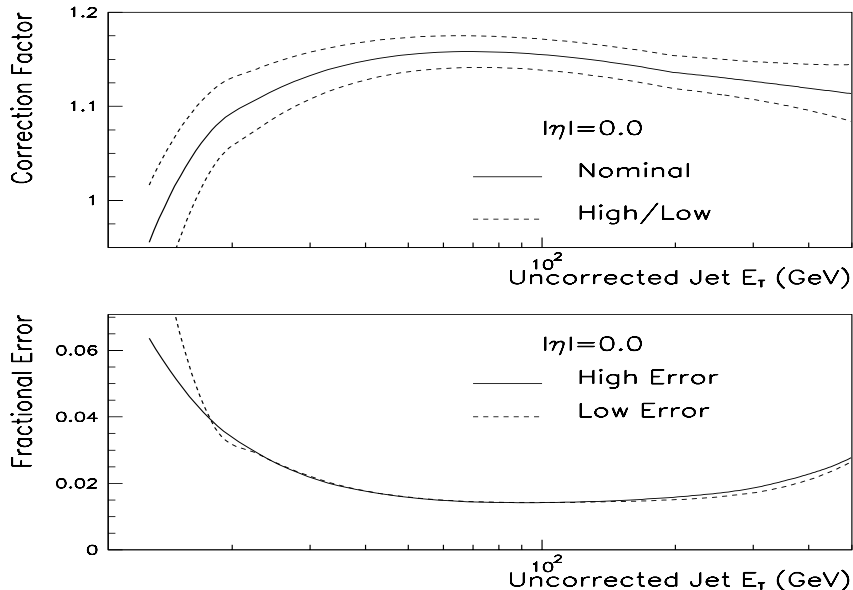


Figure 8: Jet energy correction and its error determined as described in the text for the $D\emptyset$ calorimeter.

a Monte Carlo simulation of the analysis yields good agreement. To achieve this agreement the single particle responses from test beam data were inserted directly, in similar fashion to the CDF primary analysis. The effects of leakage of particles, and hence energy, out of the back of the calorimeter has been estimated using a variety of data. It is negligible at low energies and increases to about 1% at about 400 GeV.

With \mathcal{S} , \mathcal{O} and \mathcal{R} in hand, the corrections to the jet energy scale are exhibited in Fig. 8. The upper plot shows the correction itself and the lower the associated errors which we see are less than about 2% for a considerable range in transverse energy.

The manner in which the actual calibration is extracted means that, as in the case of CDF, the uncertainties are correlated from point to point as a function of transverse energy. One such source of correlation is the use of a smooth function to fit and extract the hadronic response from the photon jet data displayed in Fig.7. With a limited number of parameters describing the fit, the uncertainties at two different energies are closely correlated while those for energies far apart are less so. In order to permit the optimal use of this information, $D\emptyset$ has constructed a complete co-variance matrix for the energy scale measurement. This is then used in conjunction with any desired data distribution to allow the construction of a full χ^2 test.

4 Physics with Single Jets

Some excitement was generated when CDF published[11] their inclusive jet cross section. In Fig. 9 we show the relative difference between the data and the theory predictions as a function of transverse momentum. In this case the theory uses CTEQ3M parton distribution

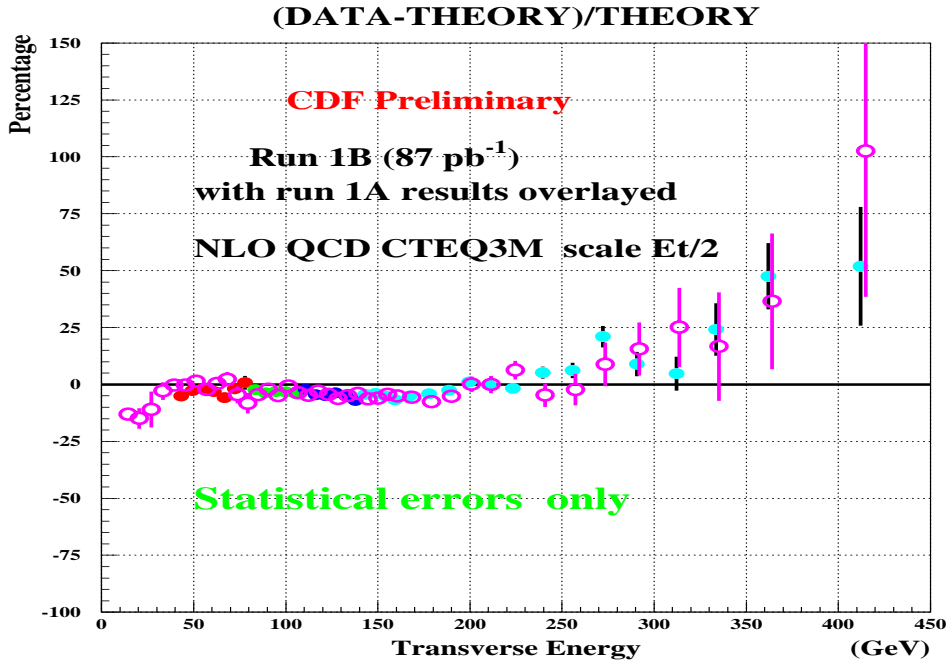


Figure 9: Inclusive jets spectrum from CDF as compared to predictions obtained using the CTEQ3M parton distributions.

functions, There is superb agreement between 50 GeV and 250 GeV over which range the cross section falls by several orders of magnitude, but at high transverse energy there appears to be a tendency for the data to rise relative to the predictions. In their publication CDF used a Monte Carlo method to compare with theory using several different parton distributions. They took into account the rather extensive knowledge of the correlations between the uncertainties on the individual data points. CDF found that the probability for the theory, to describe the data was in general not good. For MRSD0', which has similar behaviour to CTEQ3M, they found that while the agreement was good (80%) at low E_T it was only 1% at high E_T . CTEQ2M gave better agreement (more than 8%) at high E_T but did worse (23%) at low E_T . The preliminary results from their later high statistics measurements[7] confirmed the general behavior observed in the earlier data.

The rise at high transverse momentum relative to the predictions led to a variety of speculations ranging from the presence of new physics beyond QCD, which would have been very exciting, to the need to modify the parton distributions to accomodate the difference. The preliminary $D\bar{O}$ measurement available at that time showed no indication of the anomalous behaviour but could not rule quantitatively on the issue

Following the work, described above, to improve the calibration of their jet energy scale, $D\bar{O}$ recently submitted the results[12] shown in Fig. 10. There is no apparent deviation from the predictions of QCD.

A quantitative comparison of the $D\bar{O}$ data with the best fit to the CDF data shows that the latter is an unlikely description of the $D\bar{O}$ data. This comparison is made with a χ^2 test taking account all the correlations between the errors in the $D\bar{O}$ data but including no CDF errors. This is a way of stating that the $D\bar{O}$ data do not support the central trends of the

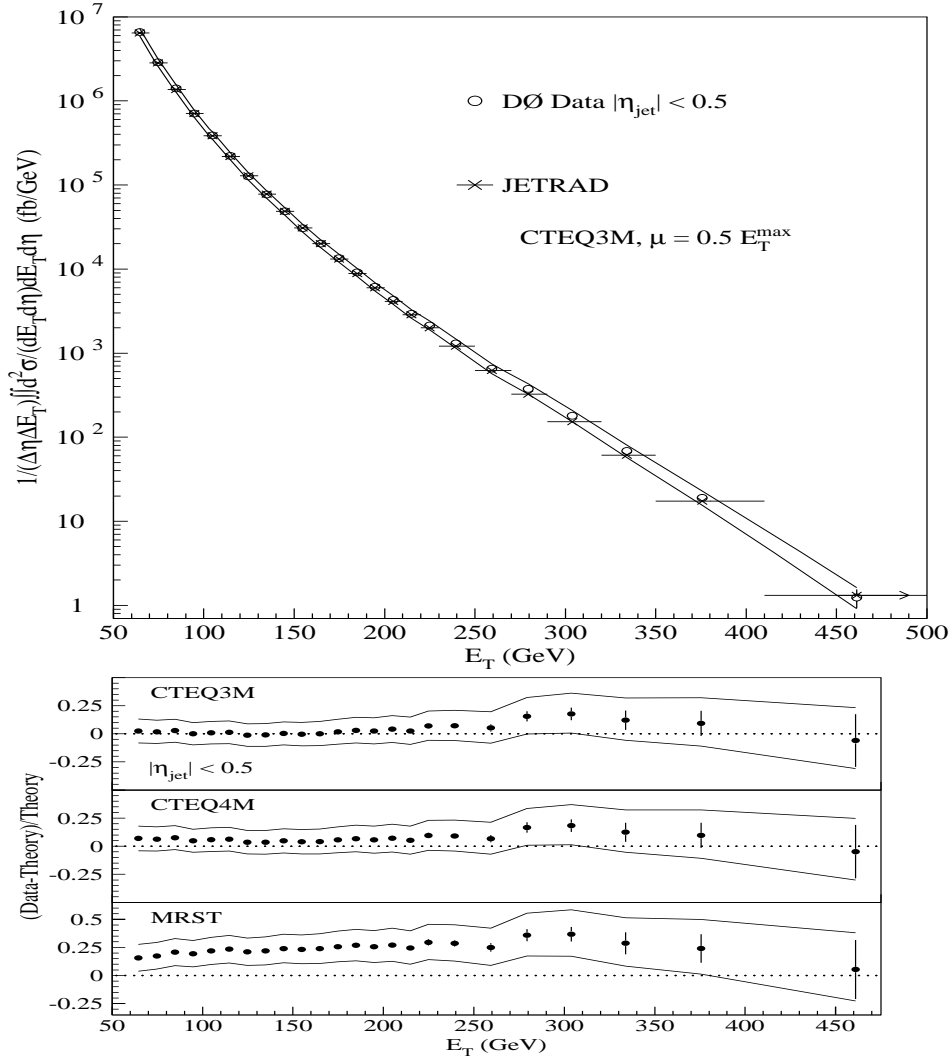


Figure 10: DØ inclusive jets cross section and a comparison with various predictions.

CDF data, including for example, a rise at high E_T with respect to the theory. Nevertheless, it must be emphasised that when the two measurements themselves are compared, taking into account the correlation matrices of both, the χ^2 test of whether the two are compatible is perfectly acceptable.

We should note that the extent to which incisive statements can be made is critically dependent on the understanding of the calibration, its uncertainties and the correlations between those uncertainties. The data fall by approximately seven orders of magnitude between 50 GeV and 450 GeV and we are discussing effects at the level of 30%. With higher luminosity data in future running and with as good or better systematic errors, we can extend the range of the measurement by about 100 GeV in E_T .

5 Physics with Multi-Jet Systems

The measurement of the spectrum of single jets described above is the most basic of possible measurements. However within the parton model, one expects any single jet observed in an event to be balanced by other jets. Given the QCD radiation of gluons, and in turn the splitting of the gluons into quark-antiquark pairs, one expects more than two jets in some fraction of events. Below we discuss first the dijet event measurements, of mass and angular distributions, and proceed to events with three, four, five and six distinct jets in the final state. To close this section we mention the production of jets in diffractive processes.

5.1 Compositeness

If the partons are composite[13], and if the possible constituents, sometimes called preons, interact via the exchange of particles with a very high mass(the compositeness scale), there is still a contribution at much lower energy scales which can be generically described by a contact interaction(a four-fermion vertex). The presence of such an interaction leads to modifications relative to the QCD predictions for several observables; these include the dijet angular distribution and the dijet mass distribution. At a later point we will also consider compositeness in as much as it affects the production of lepton pairs, the Drell-Yan process.

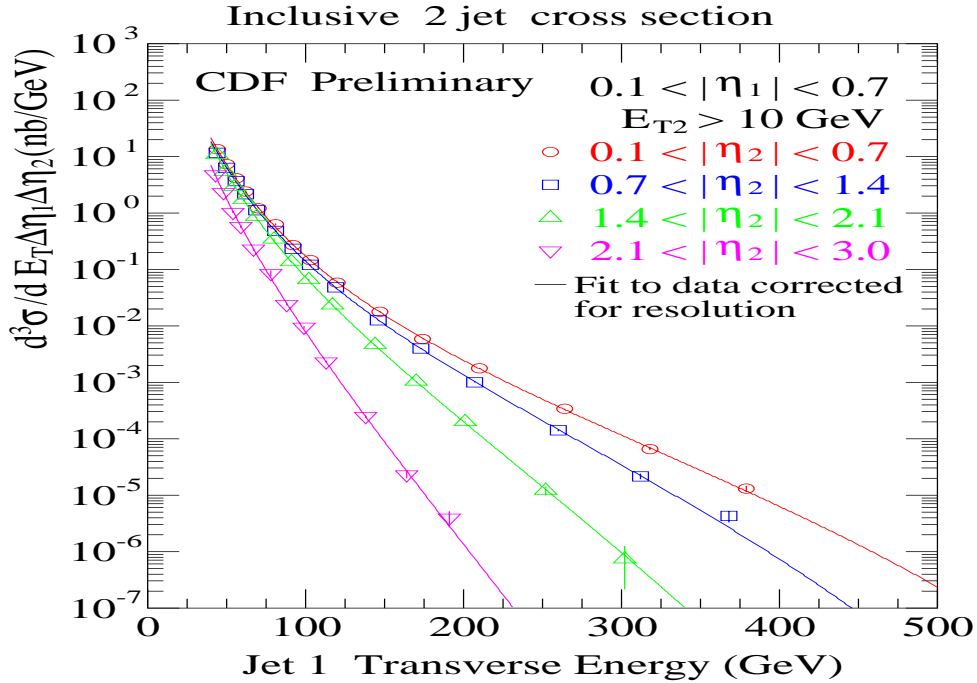


Figure 11: Dijet triple differential cross section as measured by CDF.

5.2 Dijet Cross Sections

If we measure two jets in the final state we have sufficient information to fully reconstruct an interaction with two initial state and two final state partons. The cross section as function

of the second jet kinematics, transverse energy, E_T , and pseudorapidity, η , is sensitive to the initial parton distributions at different values of the fractional momentum, x . In the CDF measurements[14] shown in Fig 11 the cross section is plotted for the case of one jet constrained to the central region. The spectra of the second jet for three different η regions out to $\eta < 3.0$ are shown along with fits to the data. The distribution becomes progressively steeper as η increases.

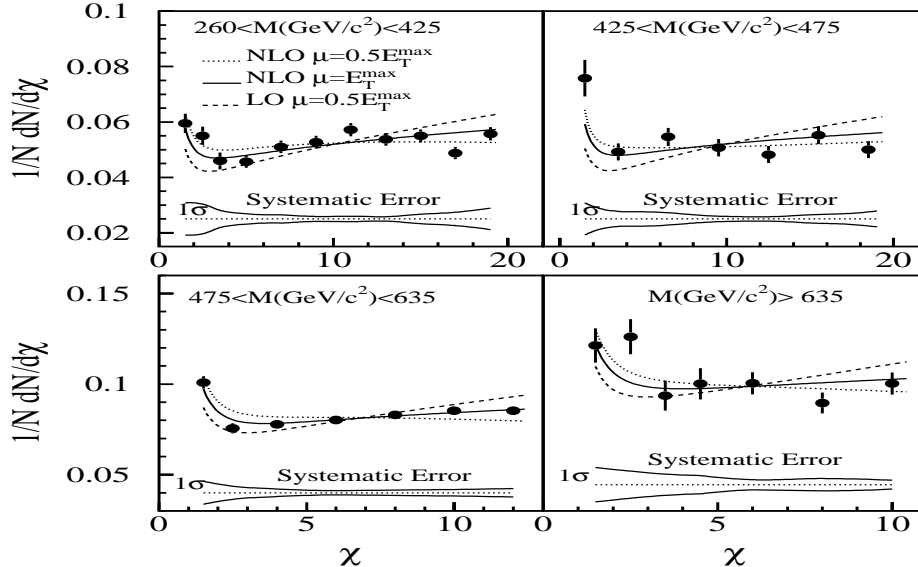


Figure 12: χ distribution as measured in the $D\bar{O}$ experiment.

5.3 Dijet Angular Distributions

The production of two final state partons proceeds predominantly through the t-channel exchange of a gluon. These processes therefore have rather similar angular distributions[1], with a peak near $\cos(\theta^*) = 1$ in the centre of mass very similar to Rutherford scattering. A transformation to the variable χ using $\chi = (1 + \cos(\theta^*)) / (1 - \cos(\theta^*))$ yields a relatively flat function, with some slight deviation due to the scale breaking effects of QCD. A contact term modifies the angular distribution by adding a term in $(1 + \cos(\theta^*))^2$ which would manifest itself as a rise at low χ . The measurements[15, 16] from CDF and $D\bar{O}$, shown in Fig. 12, are in good agreement with the next-to-leading order QCD calculations. In fact the measurements rather clearly disfavor the leading order description.

The good agreement with the next-to-leading order QCD predictions and the absence of an abrupt rise at low χ suggest that any contributions from contact interactions are small. By looking at the ratios between the cross sections in the high and low χ regions, and thereby minimising the uncertainties in the QCD predictions, for example from choice of scale, lower limits are set on the compositeness scale, Λ , of about 2 TeV.

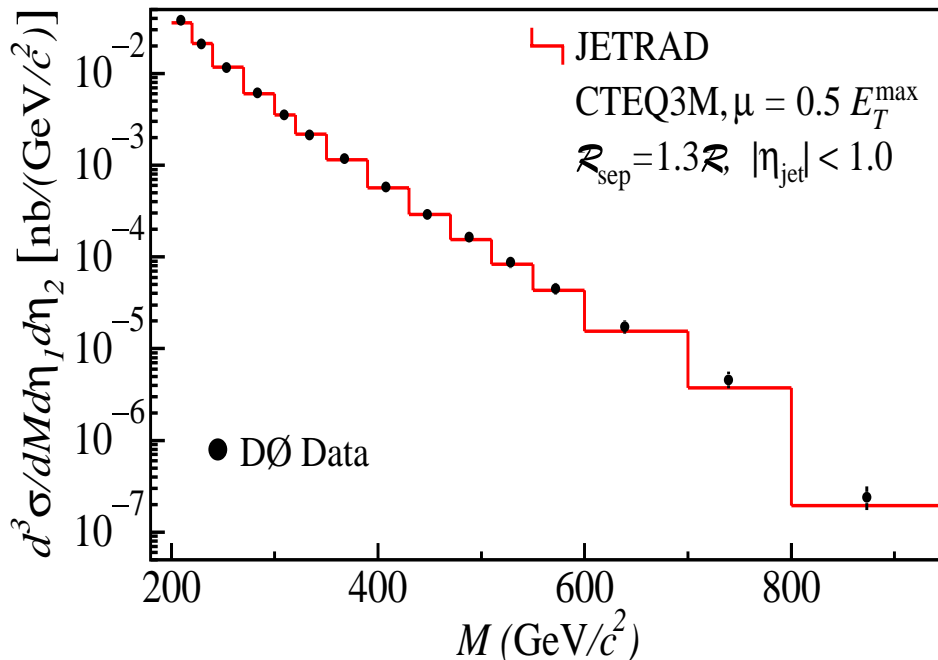


Figure 13: Dijet mass cross sections measured by the DØ experiment.

5.4 Dijet Masses

We can explicitly look at the spectrum of dijet masses either for an indication of a bump indicating a resonance or for an excess at large mass. However, any search for bumps or deviations depends on first establishing how well QCD describes the data. In Fig. 13, we see that indeed the spectrum as measured[17] by DØ is well described by QCD for masses up to 900 GeV in the central region.

By examining the behavior of the dijet mass spectra in two different η ranges, the sensitivity to possible contact interactions is enhanced. In particular the ratio is insensitive to the various uncertainties in the QCD predictions. Further the contact interactions tend to be more central than the QCD interactions. The data displayed in Fig. 14 constrain the possible contact scale to be above 2.5 or 3 TeV depending on details of the postulated higher scale interactions.

5.5 Higher Jet Multiplicities

As mentioned earlier, high multiplicities of partons in the final state imply the same high order of QCD calculation. Complete calculations are not available beyond “Next-to-Leading”, however tree level calculations are available. It is also possible to argue that the loop effects may not be so large in certain regions of phase space. Typically predictions are made using the NJETS[18] program which contains the complete matrix element, or with HERWIG[19] which contains the parton shower representation of QCD. As a contrast, the data are often compared with a “phase space” calculation which has a smooth matrix element which contains none of the co-linear singularities which characterise QCD.

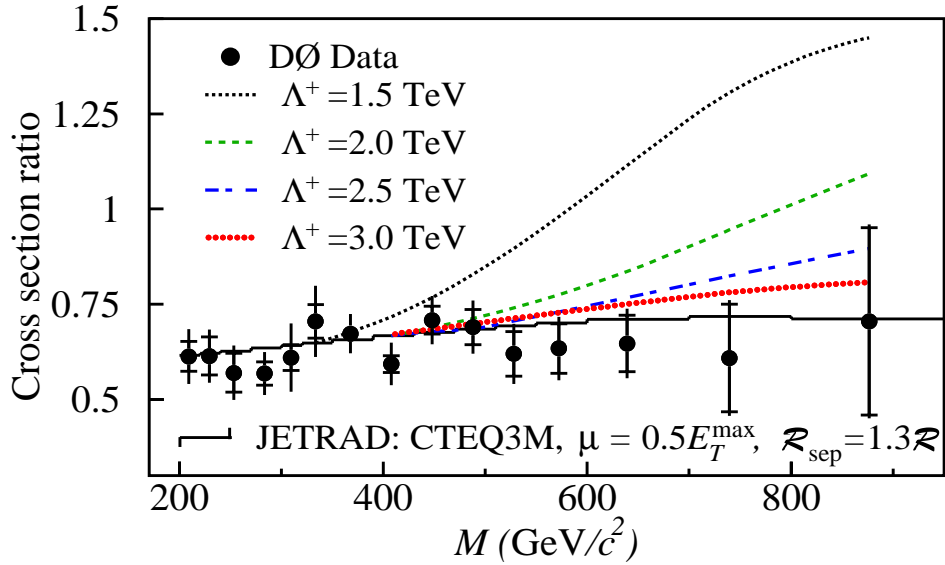


Figure 14: Ratio of the dijet mass cross sections in two different η regions measured by the DØ experiment.

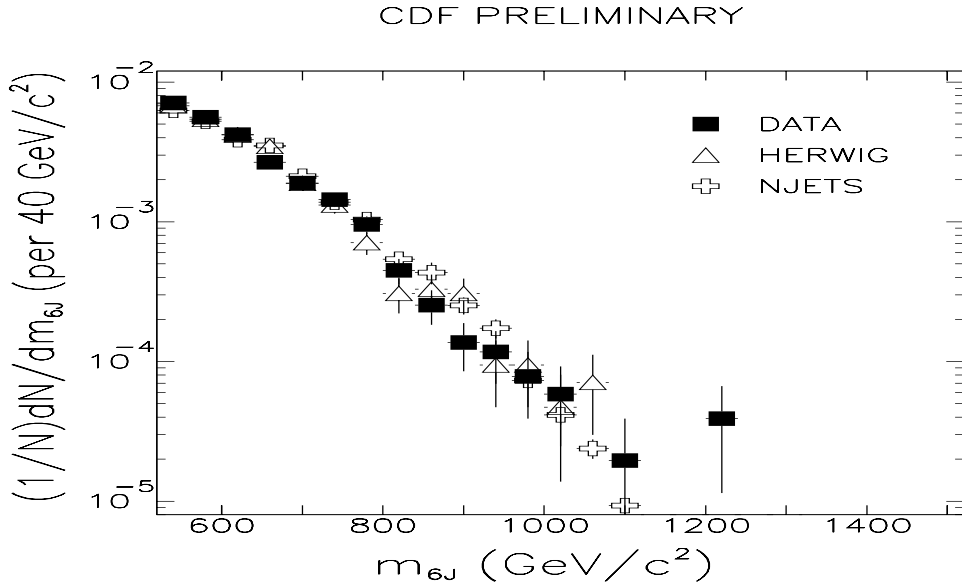


Figure 15: The distribution of events in terms of the six-jet mass above 500 GeV from CDF.

CDF has performed analyses[20] of multijet final states, most recently[21] with jet multiplicities as high as six. The distribution of 6-jet mass is shown in Fig. 15 and we see that it extends somewhat beyond the distribution of dijet masses shown earlier. The implication is that the initial state partons are carrying more than half the nucleon momenta in these regions. The distribution is well described by both the HERWIG and NJETS calculations.

The total mass might be considered to be a simple characteristic for the events. With six jets in the final state it is clear that the description is involved with a large number of parton momenta and interparton angles. However CDF finds that essentially all the different

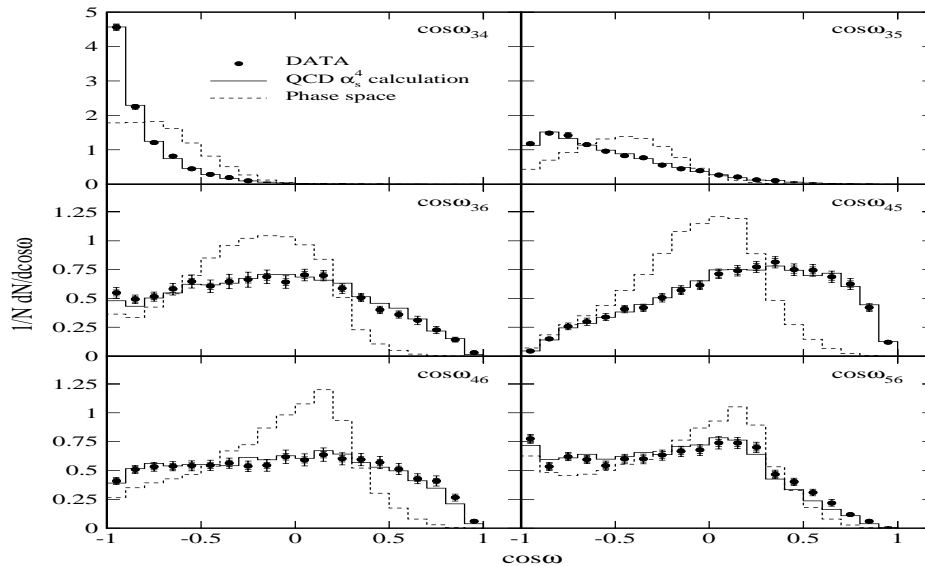


Figure 16: Distributions in terms of the inter-jet angles in events with four jets in the final state from the DØ experiment.

distributions are similarly well described. Fig. 16 shows the data distributions[22] from DØ as a function of the different interjet angles ω_{ij} where i,j are the parton/jet indices running from 3 to 6. The events have four final state jets which are ordered by transverse energy. Thus, for example ω_{34} is the opening angle between the two highest E_T jets(the labels 1 and 2 are used for the initial state partons) . Again the data are compared with the predictions of the full matrix element calculation and with a phase space description. The latter fails spectacularly while all the relevant features appear to be present in the QCD calculation.

5.6 Diffractive Jets

We are most used to dealing with jets in systems which can be described by perturbative QCD, which involve partons. However, jets also appear in classes of events which are often considered to be examples of soft interactions, for example diffractive events. In recent years an extensive cottage industry of physics associated with rapidity gaps[23] has evolved. These rapidity gaps are interpreted as resulting from the exchange of colorless objects from which there is none of the usual color radiation. The obvious candidate for such an exchange is the pomeron, the vacuum like state which was used extensively in the description of elastic and diffractive processes, thirty years ago.

Both CDF and DØ have a number of publications[24, 25] covering the subject. Here we limit our description to the event displays shown in Fig. 17. All the events display the energy deposited in the cells of the first, electromagnetic layer of the calorimeter in the DØ experiment where an energy deposit of 200 MeV is clearly distinguished from noise. The upper event is a typical event with a number of clusters of energy (jets) present and smaller clusters or individually occupied cells in the regions between the jets, and the beam remnants at high $|\eta|$.

DØ Dijet Events: η - ϕ Legos

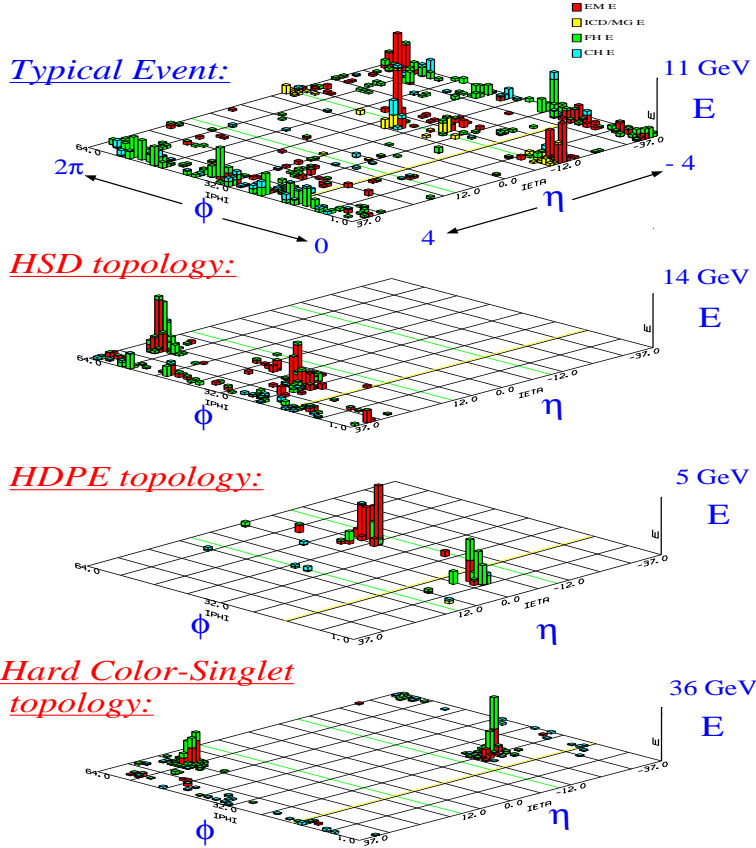


Figure 17: Examples of event displays in which characteristic topologies are evident, a normal event and three events with single diffractive, double pomeron and a central gap configurations.

The second event is dramatically different. Two jets are identifiable in a limited range of η . The absence of particles over much of the η range is suggestive of a *diffractive event*. The anti-proton has been excited and within that system two jets are produced while the recoiling proton remains unexcited.

The third event has two jets in the central rapidity region and no occupied cells, i.e. gaps, on each side in η . We would label such an event as *double pomeron* like. The gaps on either side in this case each are identified with pomeron exchange and the two jets are produced in the central region as a result of the pomeron-pomeron interaction. Hence - study of such processes offers the hope of understanding pomeron structure (indeed whether it is an object in any real sense at all) since the energy transfer to produce jets must be large - “deep inelastic” pomeron scattering.

Finally, in the bottom event we see two jets widely separated from each other in η with particles at higher η but nothing between them. This indicates a colorless exchange but in the middle of the available rapidity region.

6 The Drell-Yan Process

Quark and anti-quark constituents of the initial proton and anti-proton may annihilate forming a virtual photon which in turn produces a lepton-antilepton pair. This is known as the Drell-Yan process. As energies have increased the name has been taken to include the same s-channel production mechanism but generalized to encompass the very similar Z -boson production which again leads to charged lepton pairs in the final state. A further generalization also leads to the description of the production of a charged lepton plus its neutrino. In the case of photon and Z -boson there is clearly the opportunity for the two diagrams to interfere except exactly at the Z -pole where the resonance has an entirely imaginary amplitude while the amplitude for the photon process is real.

Within the context of these lectures we derive our interest from what the measurement of these processes can tell us about compositeness. The same arguments advanced earlier concerning the contributions of higher mass compositeness are valid here. The caveat is that both the quarks and the leptons involved should have some of the “preons” in common.

In Fig. 18 data[27] from CDF are shown in which both electron and muon pairs are combined. We see quite clearly the peak at the Z mass and the steep fall out to 500 GeV in mass. Also shown on the plot are the expectations from the Drell-Yan process itself including the interference between the photon and Z diagrams. The agreement with the data is impressive. Theoretical curves are also shown for two example compositeness calculations. Each involves a compositeness scale of 2 TeV with opposite signs for the interference terms between the Drell-Yan and the compositeness graphs. It is clear that neither of these possibilities can be accommodated by the data and so they are excluded. As the compositeness scale is increased the deviation from the Drell-Yan curve decreases and at some scale the data cannot distinguish the two. The scales excluded are in the range 2.5–5.2 GeV depending on the details of the couplings.

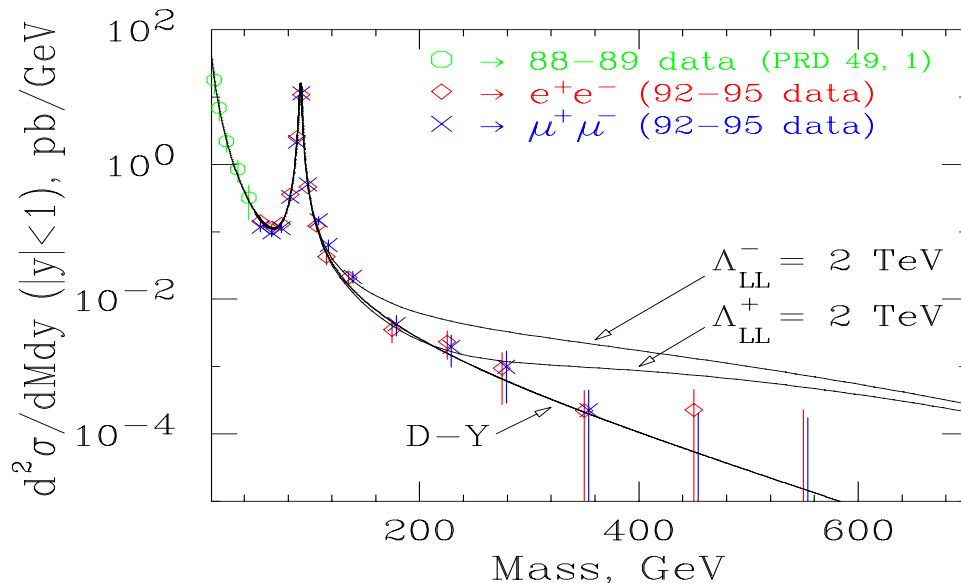


Figure 18: Drell-Yan as measured in the CDF experiment .

Recent $D\bar{O}$ data[28] are shown in Fig. 19. These data contain only electrons in the final state but they extend to higher η by using data from the $D\bar{O}$ end calorimeters. A similar analysis to that of CDF leads to slightly improved limits ranging from 3.3 TeV to 6.1 TeV, again depending on the details of the interaction Lagrangian.

7 Jets with Electroweak Bosons

Vector boson production is described in lowest order QCD by the Drell-Yan process, where two quarks annihilate. Higher order corrections due to gluon emission impart transverse energy to the vector boson and eventually at high E_T result in distinguishable jets. We consider these two effects in turn in this section.

7.1 Vector Boson Transverse Momenta

The transverse momentum spectrum of W bosons as measured[29] by $D\bar{O}$ is shown in Fig. 20. The data peak at $E_T \simeq 2$ GeV. The turnover at lower transverse energy is due to the Jacobian($dp_T^2 \simeq p_T.dp_T$). An incisive measurement of the shape in this low p_T region would be very valuable in understanding whether the current descriptions[30] which involve resummation of lots of higher order gluon emission are valid or not. For these W data the resolution at low p_T precludes a definitive judgement. Z boson data are needed.

At higher p_T there is a steady fall of the spectrum which the theory seems to follow. $D\bar{O}$ has represented the theory as a band between two solid lines which are actually the limits on the systematic variation possible as a result of the systematic uncertainties. They choose to apply their systematic uncertainties to the theory rather than to unfold the data. The agreement is reasonable although at high momenta there is a slight tendency for the theory to be below the data.

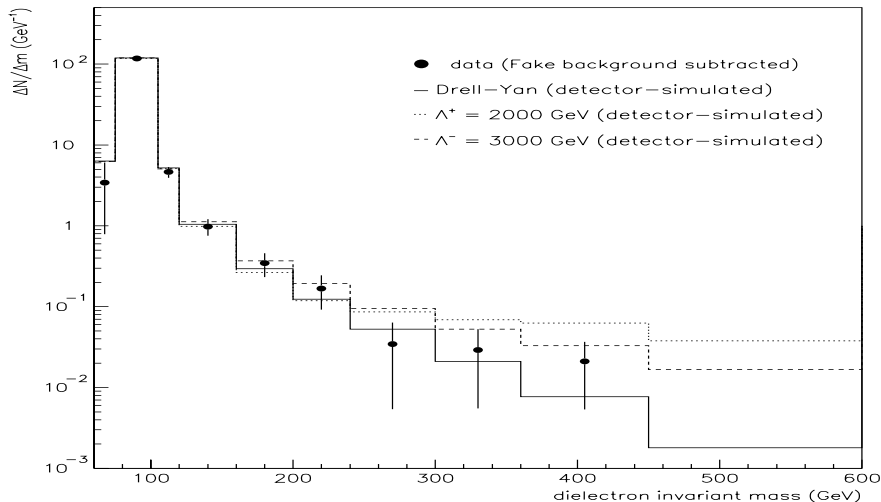


Figure 19: The Drell-Yan spectrum as measured in the $D\bar{O}$ experiment.

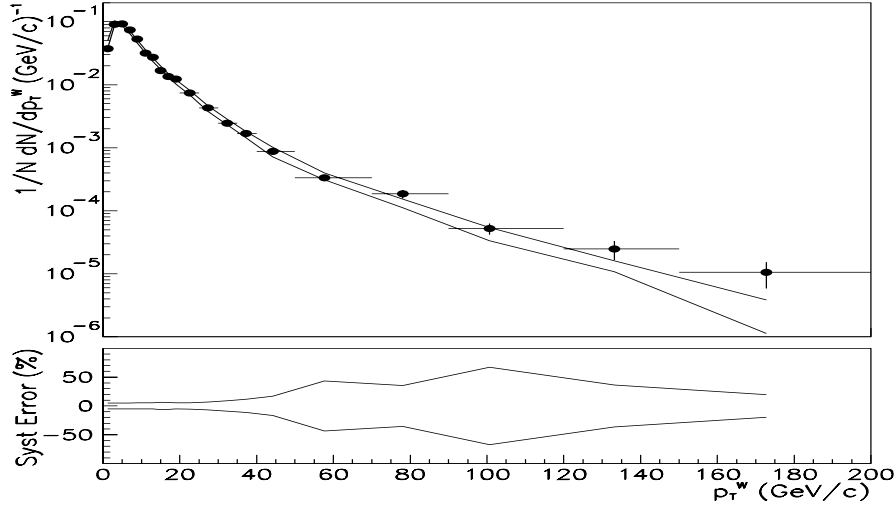


Figure 20: Spectrum of W -boson transverse momenta as measured by the DØ experiment.

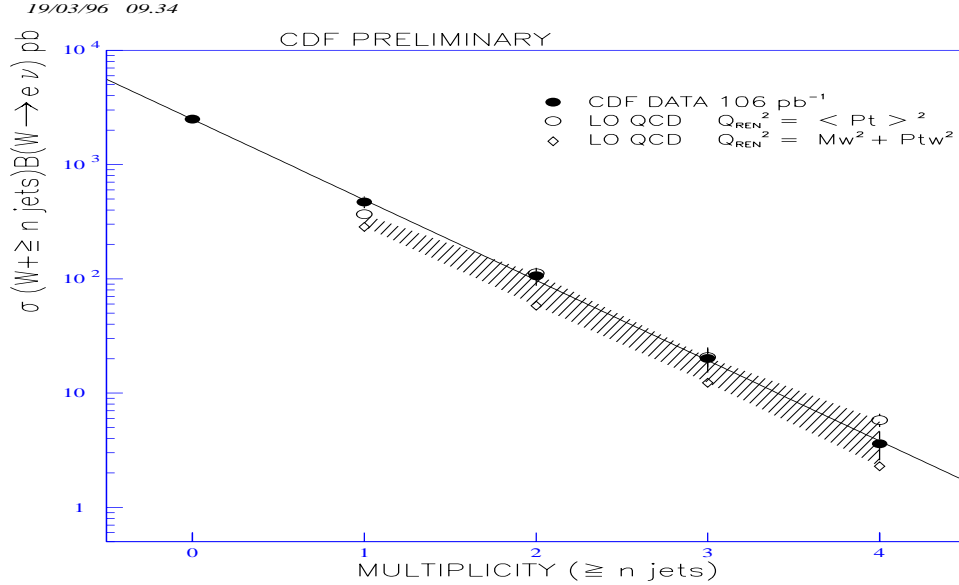


Figure 21: W + jets observed in the CDF experiment compared to leading order QCD predictions.

7.2 Vector Bosons and Jets

At higher p_T , the transverse momentum of the vector boson manifests itself explicitly in the jets produced in the event. In Fig. 21 we display the inclusive multiplicity[31] distribution for jets in events with a W boson. The approximately exponential decrease as a function of multiplicity is driven by the extra factor of α_S , the QCD coupling constant, which appears each time the number of jets is increased by one. The leading order theory expectations are represented as a band which lies slightly below the theory. The boundaries of the band

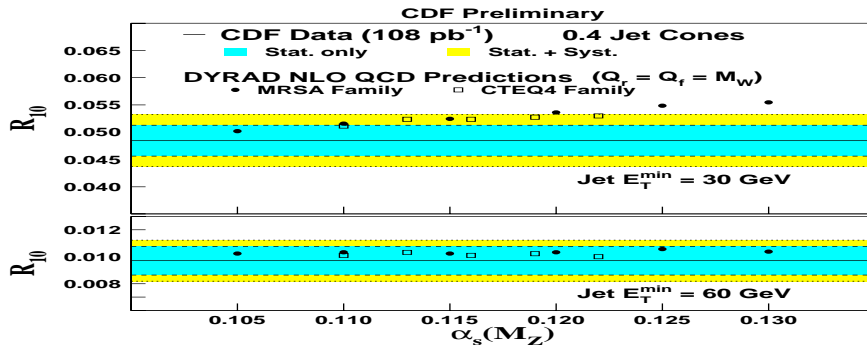


Figure 22: $R_{10} = N_{events}(W + \geq 1jet)/N_{events}(W + \geq 0jet)$ in the CDF experiment compared to leading order QCD predictions.

are given by the leading order calculations with two different scales: one is the p_T^2 of the W , the other is $M_W^2 + p_T^2$. The importance of comparisons such as this, and indeed of the understanding of the data, is increased when we remember that a process such as $t\bar{t}$ production results in a W -boson and four jets in the final state. Thus, the QCD process, which we study in this section is a dominant background in one of the most important top production channels.

This idea that the multiplicity is driven by α_S suggests that a careful measurement of the ratio between the numbers of events with one or more jets, compared to the total, $R_{10} = N_{events}(W + \geq 1jet)/N_{events}(W + \geq 0jet)$ should be sensitive to α_S . This quantity was measured by UA2[32] and more recently[33] by DØ. The agreement with the next to leading order theoretical calculation in the DØ measurement left something to be desired. A recent measurement[34] by CDF is displayed in Fig. 22. Agreement with the theory is very good; however the sensitivity to α_S is disappointing.

8 Jet Spectroscopy

The reconstruction of an intermediate state which decays into the particles we observe has been a tool that has served particle physics well. To cite but one example, the Z boson was observed through reconstructing and observing a peak in the mass spectrum of lepton pairs. Recently the top quark was observed[35]. Since the top does not exist long enough to hadronise and form a meson, its decays are to partons which appear as jets. In order to measure its mass, it was necessary to reconstruct the effective mass of the top quark using its components; the leptons and jets. Thus far this is the most sophisticated use of jet spectroscopy. We will discuss some of the salient features and difficulties.

An obvious place to start a discussion of jet spectroscopy is with the di-jet mass spectrum. We have seen that there is no obvious sign of a large *bump* indicative of a resonance. To do better we need to be more sophisticated. The line shape for the dijet decays depends on the process and must be accounted for, but the fundamental techniques remain simple: fit the spectrum to a smooth function and a suspected resonance shape taking into account all resolution effects.

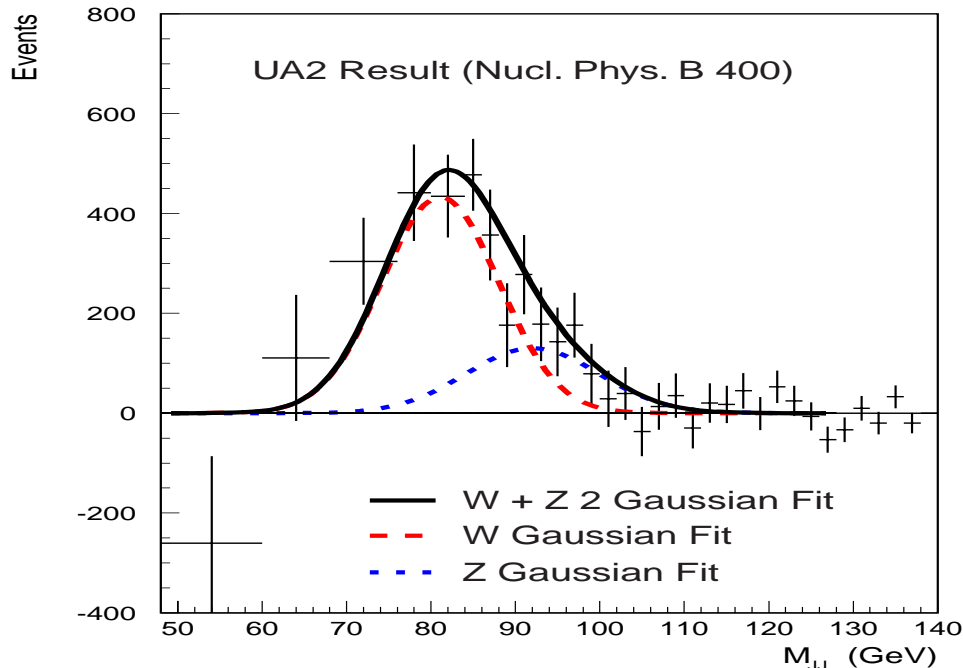


Figure 23: The effective mass distribution after background subtraction for two jets observed by UA2.

We discuss, the observation of the high mass vector bosons, the W and the Z through their hadronic decays. We then proceed to searches for higher mass vector bosons. We will spend a little time with the determination of the mass of the top and conclude with a discussion of the use of jet spectroscopy to search for the Higgs boson.

8.1 $W \rightarrow jets$

The W boson is usually detected, as it was discovered, through its semileptonic decays, which result in a distinctive isolated lepton and missing energy in the events. However, the same boson decays a larger fraction of the time to two light quarks. It is interesting to ask whether this ostensibly simple case of jet spectroscopy has any success. The measurement was attempted and completed[36] by the UA2 experiment operating at the $S\bar{p}\bar{p}S$ collider.

The difficulty with the measurement is the need to take data at masses lower than that of the resonance in order to ensure an adequate background subtraction. The rates are very high, dominated by gluon jets and uncorrelated quark jets. The dijet mass spectrum, analogous to that shown in Fig. 13, but at lower mass, shows no visible peak. However a fit to an flexible ansatz yields a rather high χ^2 to which most of the contribution comes from the region around 70-100 GeV. Removal of that region from the fit results in an acceptable χ^2 . This smooth curve is then taken as a representation of the dijet background and is subtracted from the data. The result is shown in Fig. 23. The peak corresponds well to the mass of the W -boson and the significance is in excess of 4σ .

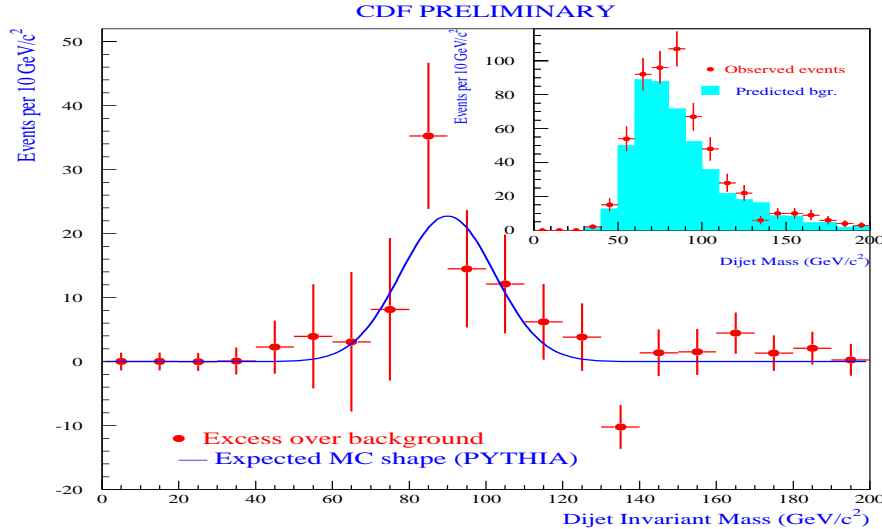


Figure 24: The effective mass distribution for two tagged b -quark jets observed by CDF.

8.2 $Z \rightarrow jets$

Recently[37], CDF has examined a data sample taken with a single central muon trigger which contains two jets. As a result of the muon trigger there is little bias on the jets which enter the trigger; it is nevertheless enriched in b -quark jets. Events are then selected in which a separated vertex tag is found for each of the two leading jets. The Z production is predominantly s -channel and therefore topological cuts on the accompanying radiation provides discrimination against generic QCD jets. For the top-quark analyses, specialised jet energy corrections have been developed for b -jets containing semi-muonic decays. These were shown to improve the mass determination both in scale and in resolution for the $Z \rightarrow b\bar{b}$ decays.

The observed distribution after the analysis is shown in Fig. 24. A hint of an enhancement is observed with a mass close to 90 GeV which is interpreted as the decay $Z \rightarrow b\bar{b}$. The signal is visually quite small; nevertheless a detailed fit establishes a signal of $90 \pm 30(stat) \pm 19(syst)$ events. The significance of the signal is between two and three standard deviations. It augurs well for the use of this decay in future data, using a displaced vertex trigger in addition to the semi-leptonic triggers to calibrate the detector for b -quark jets.

8.3 Higher mass boson searches

In 1997, the $D\bar{O}$ Collaboration examined the dijet mass spectrum considering the possible contributions from a variety of possible states that could decay into two quarks. These possibilities included an excited quark q^* , a Z' , similar to the normal Z but of higher mass and a W' , similar to the W but of higher mass. These states have somewhat different line shapes so at some level it is necessary to treat them separately. In deducing the mass limits the differences in branching fractions expected must also be considered. As an example, the results for a q^* are shown in Fig. 25. Comparison of the measured and expected cross section

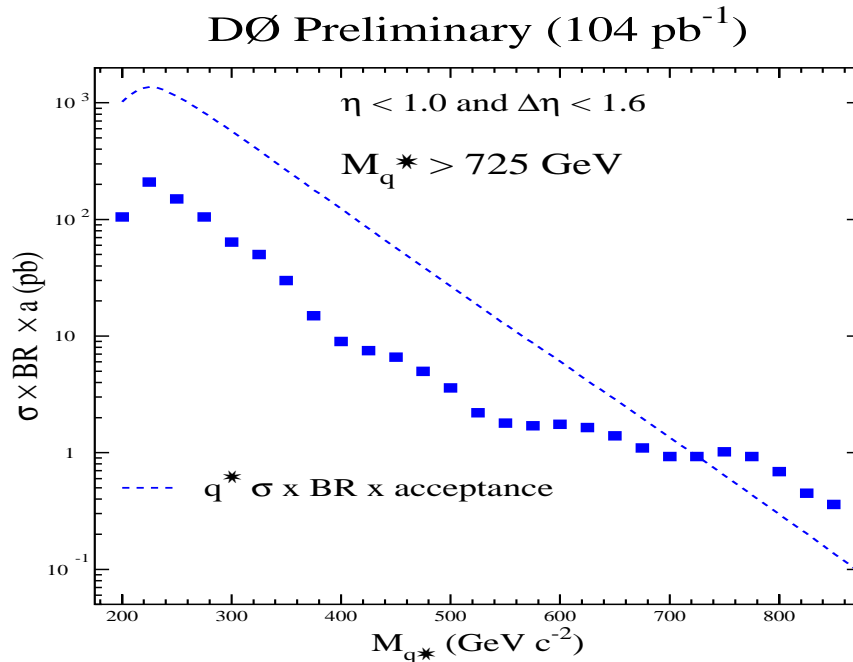


Figure 25: The 95% CL on the production cross section for an excited quark, q^* compared with the predicted cross section. Values of $M_{q^*} < 725$ GeV are excluded at the 95% CL.

at the 95% confidence level(CL) leads to a lower limit on the mass of such an object of 750 GeV. This measurement extends the limits set earlier by UA2[39] and CDF[40].

The 95% CL lower mass limits obtained in the DØ analysis also include 615 GeV for the Z' and 680 GeV for the W' . This latter is interesting in the context of the analyses[41, 42] which have set lower mass limits in the same 600-700 GeV range using leptonic final states for a number of different possible models.

Very recently both the CDF and DØ collaborations have presented searches[43, 44] for the Higgs boson and various technicolor states. In both cases one can expect finite cross sections for the associated production of a W boson and either the Higgs or the Technipion, for example. With the current luminosity the limits obtained are somewhat above the expected cross sections. Nevertheless these examples are prototypical of analyses expected to be very important in the upcoming running of the Tevatron and eventually of the LHC. One of the features is the use of lepton or displaced vertex tagging to indicate a b -quark jet in a manner analogous to the earlier mentioned CDF observation of the Z -boson decay to b jets.

8.4 Jet Spectroscopy in Top Decays

The DØ top mass measurement is published[45] as is that from CDF[8]. These measurements have been dominated by the $t\bar{t}$ decay channel of a lepton, electron or muon missing energy and four or more jets. The lepton and missing energy come from the decay of one of the W bosons; two of the four jets come from the decay of the second W boson and the final two jets come from the b quarks from the $t \rightarrow Wb$ decays. This channel gives a relatively clean signal and there are sufficient measured quantities to completely determine the t -quark mass. In

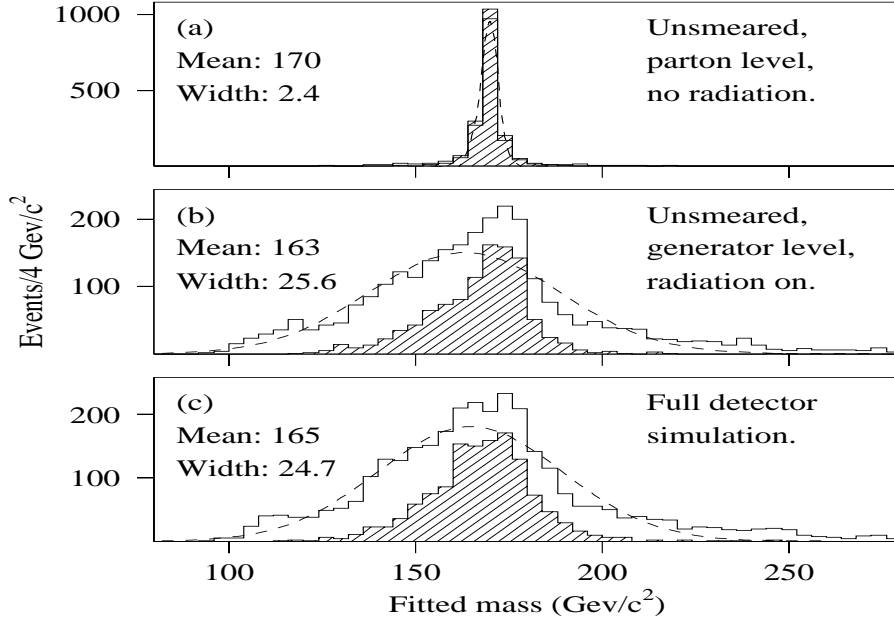


Figure 26: Monte Carlo studies of effects in the reconstruction of the top mass from QCD radiation and from detector resolution.

fact a 2-constraint fit is usually performed. While the analyses from the two groups differ in detail they both address the same issues: how to handle QCD radiation from the numerous partons in initial and final states, how to correct for energy scales which may differ from one parton species to another and how to handle the numerous possibilities for false association of objects.

The difficulties are illustrated in Fig. 26 which shows the result of a Monte Carlo study[45] by DØ of their analysis including misassignments. The upper figure shows the top mass as reconstructed from the objects at the parton level with no QCD radiation and no detector resolutions applied. The second figure indicates, in the open histogram how the rather sharp peak of the upper plot is degraded by the effects of QCD radiation from the decay and the procedure for jet assignment. The hatched histogram indicates the result when the correct assignment is made. Finally the bottom plot shows the effects of, the above problems plus incorporation of full simulation of the detector. The fact that the widths of the latter two peaks are similar, indicates the dominance of the problems of radiation.

The jet cone size is usually chosen to be somewhat smaller than that used for the QCD analyses. Usually $\Delta R= 0.4-0.5$ is the choice because, with the large number of jets in the final state, maintaining a high efficiency for the separate reconstruction of the jets is important. Since there are light quark jets and b -quark jets, specialized jet energy corrections are developed which attempt to take into account the possible difference between jet shapes and the possible loss of energy as a result of muons or neutrinos embedded in the b -quark jets. Using Monte Carlo, one also designs these corrections to yield the true parent parton energy by making a correction for the QCD radiation out of the cone. The procedure is usually checked by looking at the way the jet energies balance that of a known, well measured object

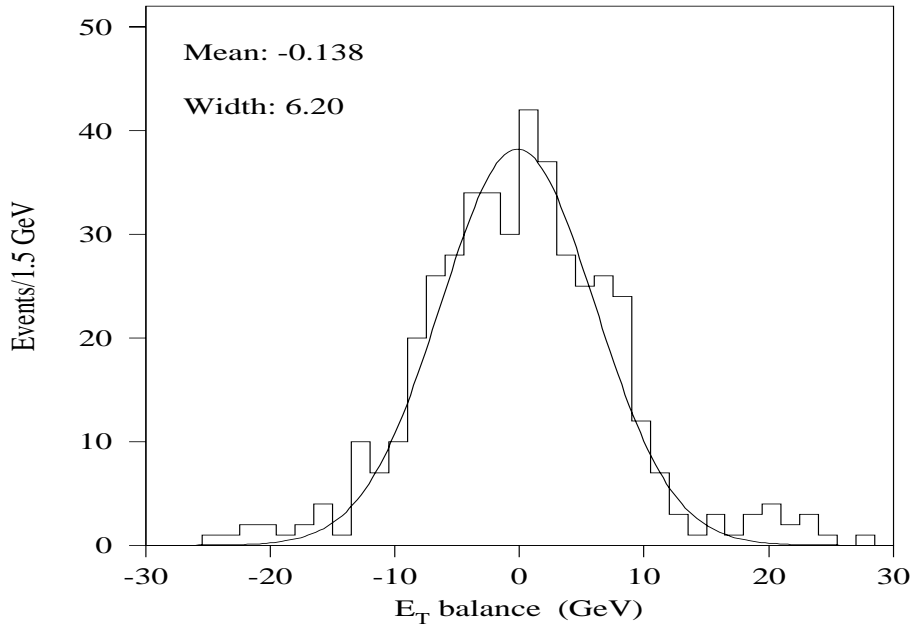


Figure 27: Transverse energy balance in $D\bar{0}$ events containing a Z boson and jets.

in some sample of events. Fig.27 shows such a check by $D\bar{0}$ using a sample of Z events with jets. Such plots are used to estimate the uncertainties in the determination of the jet energy scale.

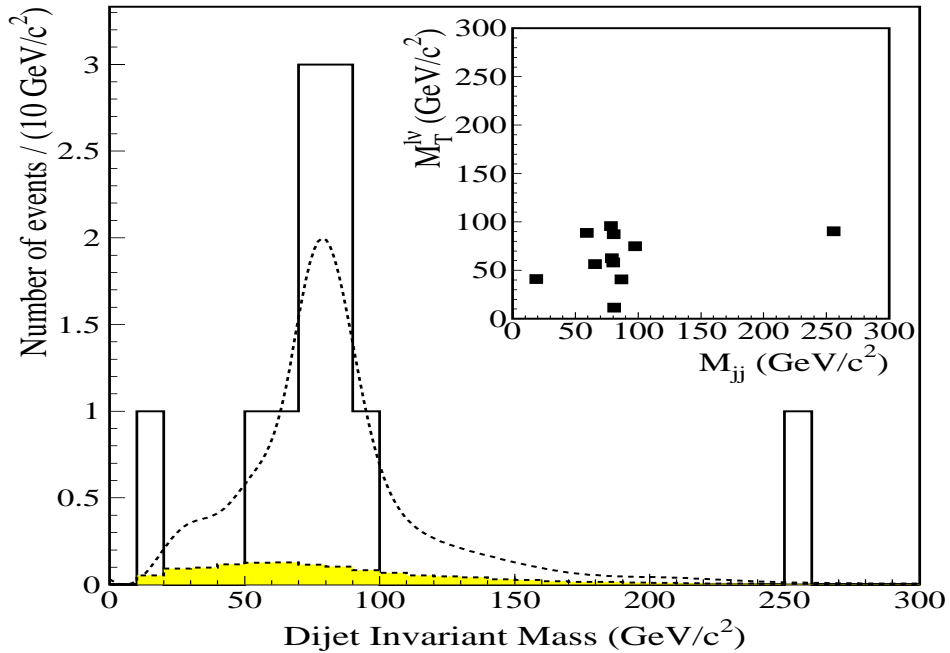


Figure 28: Light quark pair mass distribution in CDF single lepton top sample

Recently CDF has shown[46], see Fig. 28, a distribution of the effective mass of the dijet system composed of the jets assigned as the decay products of the W boson in a sample of top events. In the present primary top analyses this is applied as a constraint on the event and in this sample that constraint was relaxed. With the present data statistics limits the use of these data as a calibration of the light quark jet energy scale. However we can look forward to extensive use being made of this technique in future higher luminosity data.

In principle the $t\bar{t}$ system decays to a four jet final state in the case we are considering. However, misreconstruction can lead to the false combination of two jets, and in addition there may be extra jets, gluons, radiated both in the initial state and the final state. There have been many studies to try and develop optimal procedures but none of the clever cuts to remove jets, which are thought to be highly likely to come from initial state radiation, meets with dramatic success. In some cases a clear lepton or displaced vertex tag can clarify things and reduce the possible combinations. Beyond that restriction it is usual for all possible combinations of assignments of the jets to be considered. A judgement is then made on the quality of the kinematic fit of the total event to the $t\bar{t}$ hypothesis.

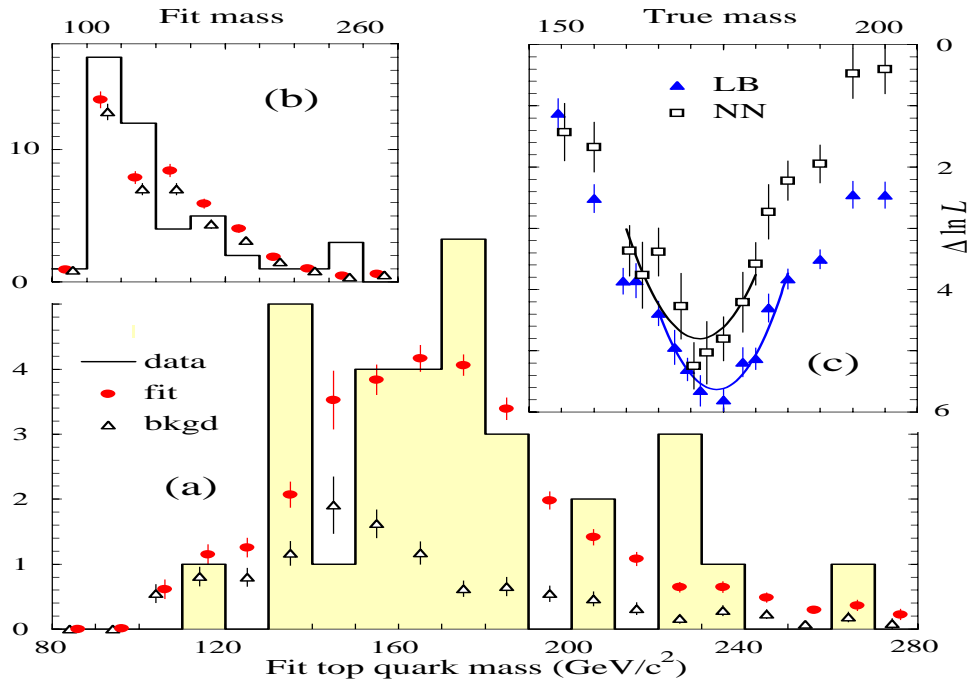


Figure 29: The mass distribution for $D0$ lepton-plus-jets $t\bar{t}$ candidates illustrating the background and the signal as well as the likelihood distributions from which the best value of the mass is determined.

Despite these difficulties the reconstruction of the mass of the top quark has been one of the success stories of high energy physics in the past few years. The analysis from $D0$ is shown in Fig. 29. After initial selection of a candidate sample the data are analysed as a function both of the top mass and of the similarity of the event to the expectations for a top event. The shaded histogram shows the apparent top mass distribution for a sample likely to be from top with the expected distribution of the background being shown as the open triangles and the signal plus background as the solid points. The inset in the top left of

the figure shows the complementary sample containing few top events. The horizontal scale in these figures is the top mass which comes out of the kinematic fits of the events. Monte Carlo studies show that this differs from the true top mass as a result of the subtleties of the procedure. Templates are therefore developed for a number of possible true top mass values and a likelihood fit to these distributions is made as a function of true top mass. The result of two variants of that likelihood fit are shown in the inset at top right of the figure. From the rather pronounced dip in the negative Log-likelihood, one can already see a good precision in top mass determination.

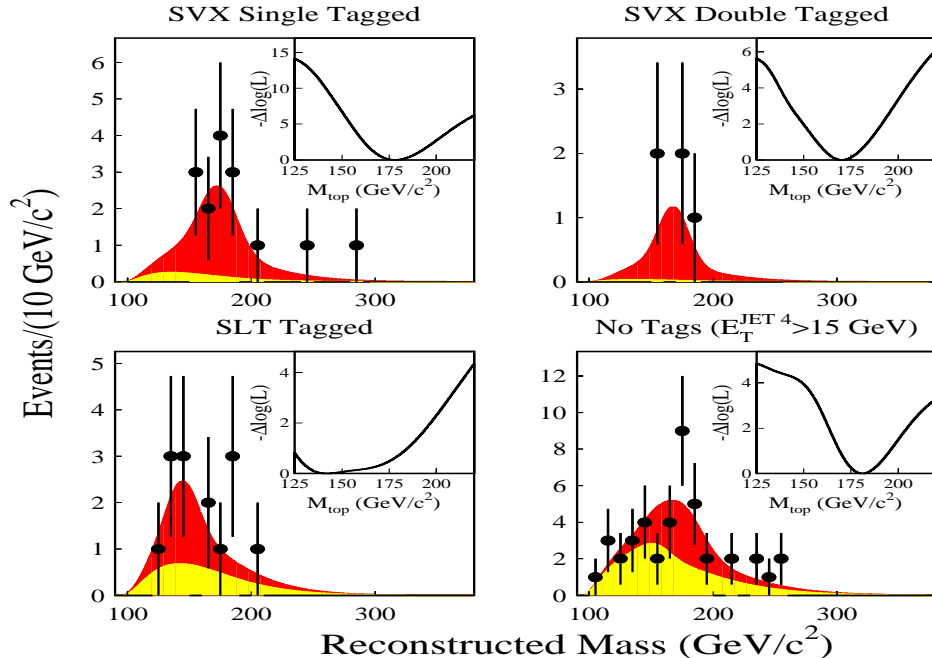


Figure 30: The mass distribution for CDF lepton-plus-jets $t\bar{t}$ candidates showing the background and the signal as well as the likelihood distributions for four different subsamples which differ by the method and extent of the b -jet tagging with the displaced vertex(SVX) and soft lepton(SLT) tags.

The results of the analogous CDF analysis are shown in Fig. 30. In their case the “quality” of the sample is assigned based on the method and extent of b -jet tagging present in the event. The subsample with two tags has the smallest background and that with no tags has the highest. The widths of the distributions and the statistics vary from sample to sample.

The resulting determinations of the top quark mass is $m_t = 173.3 \pm 5.6(stat) \pm 4.4(syst)$ from $D\bar{O}$ and $m_t = 175.9 \pm 4.8(stat) \pm 5.3(syst)$ from CDF are at the same time remarkably accurate and still dominated by the uncertainty coming from the jet energy scale determination.

Use has also been made of the dilepton events[47, 48]; in these samples the statistics are rather limited, and the constraints are fewer. Nevertheless the impact of the jet energy scale on the mass uncertainty is less (there are in general two fewer jets than in the single lepton sample). Finally while both experiments have measured the production cross section using the six jet $t\bar{t}$ final state, CDF has also determined[49] the top mass from that channel.

8.5 Higgs \rightarrow jets

Given the success of the search for the top quark and the detailed analyses of the Z and the W , we are now concentrating considerable energy on the search for the Higgs boson and possible technicolor or SUSY final states. Many, or even most, of us would like to find the Higgs boson or its equivalent.

While leptonic decays of objects tend to lead to more distinctive signatures, the observable cross section is often correspondingly low. Why not look for the decay of these higher mass objects through their decays into jets? In these lectures we have been able to demonstrate success in the use of jets for spectroscopy. The jet decays of W , Z and top are now established and well measured. Does this mean that we can rely on the technique to find the Higgs boson at the Tevatron or at LHC?

A number of studies have been made[50, 52, 51] which demonstrate the technique using Monte Carlo studies of associated Higgs production. The signals are very small, considerable luminosity is required, at least in the 10-30 fb^{-1} range (currently we are looking at data with a factor 100 less integrated luminosity). The studies[52] concentrate on the same things that concerned the top analyses, to wit, the energy scale and the assignment of jets; the initial and final state radiation problem. With the Z decays to $b\bar{b}$ jets and those of the W to light quarks the jet energy *per se* would seem to be under control. The problem really seems to be to develop a methodology to handle the initial and final state radiation and the jet recombination. While we discussed this issue with examples from Ref.[52] in the lectures, in this written version we refrain from reaching any conclusion in print since, as we write, a rather vigorous study[53] of the problem is coming to a head and we expect results of Monte Carlo studies rather soon.

9 Summary

In these lectures we have attempted to outline some of the methods for treating jets in high energy hadron collider experiments. We have seen how the measurement of jets can be used to make rather detailed investigations and measurements of the details of the strong interaction. We have also shown how jets, as manifestations of the fundamental partons produced in high energy collisions, can be combined such as to reconstruct the intermediate final states. This is analogous to the hadron spectroscopy of an earlier decade and indeed a lot of techniques were resurrected from that era. We are at a stage where jets are well established as tools and probes of high energy physics. However we do not yet have all the techniques we need. We need lots of ingenuity to learn how to best utilize the jets, the concept and the reality, to expose the underlying shape of our world.

10 Acknowledgements

In this electronic age we are used to having access at the push of a button to descriptions and diagrams produced in many parts of the world. This has greatly facilitated the preparation of these lectures. I would therefore like to thank the following people who have helped in this work either knowingly or unknowingly: Drew Baden, Iain Bertram, Jerry Blazey,

Andrew Brandt, Tom Diehl, Daniel Elvira, Brenna Flaughner, Steve Geer, Cecilia Gerber, Herb Greenlee, Carla Grosso-Pilcher, John Hobbs, Ashutosh Kotwal, Jody Lamoreux, Don Lincoln, Rob Snihur, Juan Valls, Nikos Varelas, Rich Partridge, Harry Weerts and John Womersley. I would like to thank Andrew Brandt, Gene Fisk, Brenna Flaughner, Nikos Varelas and John Womersley for reading and commenting on the manuscript. Finally the school, even if hard work, was immensely enjoyable and I would like to express my appreciation to the organisers and students.

References

- [1] R.K.Ellis, W.J. Stirling & B.R.Webber, *QCD and Collider Physics*, Cambridge University Press, 1996.
- [2] For older reviews, see for example H.E. Montgomery, CERN-EP/82-192 Presented at the Europhysics Study Conference: Jet structure from quark and lepton Interactions. Erice, Sicily, 1982. L. Di Lella, *Ann.Rev.Nucl.Part.Sci.* **33**:107-134,1985.
- [3] A. R. Baden, *Jets and Kinematics in Hadronic Collisions*. *Int. Journal. Mod. Phys.* A(1998).
- [4] See for example J. Drees & H.E. Montgomery, *Ann. Rev. Nucl. Part Sci.*, 1983 **33**: 383; H.Eugene Fisk & Frank Sciulli, *Ann. Rev. Nucl. Part. Sci.* 1982. **32**:499, 1982; T. Sloan, R. Voss , G. Smadja (Saclay) *Phys. Rep.* **C162**:45-167, 1988.
- [5] Brenna Flaughner, Karlheinz Meier in proceedings of Research Directions for the Decade, Snowmass 1990, pp 128-133, Ed. E. L. Berger (World Scientific, 1992); J. Huth *et al. ibid.* pp 134-136; B. Abbott *et al.* FERMILAB-CONF-97-325-E.
- [6] S. Catani, Yu. L. Dokshitzer, M.H. Seymour & B.R. Webber, *Nucl. Phys.* **B406** (1993), 187.
- [7] Brenna Flaughner, CDF Collaboration, Joint Experimental and Theoretical Seminar, Fermilab, February, 1996.
- [8] F. Abe *et al.*, CDF Collaboration,*Phys. Rev. Lett.* **80**, 2767 (1998); *Phys. Rev.* **D50**, 2966 (1994).
- [9] B. Abbott *et al.*, DØ Collaboration,FERMILAB-PUB-97/330-E, hep-ex/9805009, to be published in *Nucl. Instr. Meth. Phys. Res. A*.
- [10] H. Schellman, The relation between the E_T Asymmetry, Jet Resolutions and Vertex Resolution, DØ Note 3454, 1998.
- [11] F. Abe *et al.*, CDF Collaboration, *Phys. Rev. Lett.* **77**, 438 (1996).
- [12] B. Abbott *et al.*, DØ Collaboration, FERMILAB-PUB-98/207-E ,hep-ex/9807018, submitted to *Phys. Rev. Lett.*
- [13] E. Eichten, K. Lane and M. Peskin, *Phys. Rev. Lett.* **50**, 811 (1983); E. Eichten, I. Hinchliffe, K. Lane, and C. Quigg, *Rev. Mod. Phys.*, **56**, 4, 1984.
- [14] J. Lamoureux, CDF Collaboration, FERMILAB-CONF-98/315-E. Proceedings 29th International Conference on High Energy Physics (ICHEP 98), Vancouver, British Columbia, Canada, July 23-30, 1998.
- [15] F. Abe *et al.*, CDF Collaboration, *Phys. Rev. Lett.* **77** 5336 (1996);Erratum *Phys. Rev. Lett.* **78** 4307 (1997) .

- [16] B. Abbott *et al.*, DØ Collaboration, Phys. Rev. Lett. **80** 666 (1998).
- [17] B. Abbott *et al.*, DØ Collaboration,FERMILAB-PUB-98/220-E, hep-ex/9807014, submitted to Phys. Rev. Lett.
- [18] NJETS: F. A. Berends, W. Giele, and H. Kuijf, Nucl. Phys. **B333**, 120 (1990).
- [19] HERWIG: G. Marchesini *et al.*, Comp. Phys. Commun. **67** (1997) 465.
- [20] F. Abe *et al.*, CDF Collaboration, Phys. Rev. Lett. **75**, 608. (1995); Phys. Rev. **D54**, 4221 (1996).
- [21] F. Abe *et al.*, CDF Collaboration, Fermilab-PUB-97/093-E, 1997, submitted to Phys. Rev. D..
- [22] S. Abachi *et al.*, DØ Collaboration, Phys. Rev. **D53** 6000(1996).
- [23] A. Brandt, Hard Diffraction and Rapidity Gaps, Proceedings *15th International Conference on Physics in Collision*, Cracow, Poland, June 8-10, 1995.
- [24] F. Abe et al., CDF Collaboration, FERMILAB-PUB-98/334-E. Submitted to Phys. Rev. Lett.; Phys. Rev. Lett. **79**. 2636 (1997); Phys. Rev. Lett. **78**, 2698 (1997); Phys. Rev. Lett. **80**, 1156 (1998);Phys. Rev. Lett. **74**, 855 (1995).
- [25] B. Abbott *et al.*, DØ Collaboration, Phys. Lett. **B 440**, 189 (1998); B. Abbott *et al.*, DØ Collaboration, Hard Diffraction in $\bar{p}p$ Collisions at $\sqrt{s} = 630$ and 1800 GeV, Paper #469, Submitted to the *XXIX International Conference on High Energy Physics - ICHEP98*, July 23-29, 1998, Vancouver, B.C., Canada; S. Abachi *et al.*, Phys. Rev. Lett. **76**, 734 (1996); Phys. Rev. Lett. **72**, 2332 (1994).
- [26] see for example C. Grosso-Pilcher and M.J. Shochet, Ann. Rev. Nucl. Part. Sci. **36** 1986:1.
- [27] F. Abe et al., CDF Collaboration, Phys. Rev. Lett.**79** 2198 (1997).
- [28] B. Abbott *et al.*, DØ Collaboration, Fermilab-Pub- xxx, submitted to Phys. Rev. Lett, Dec, 1998.
- [29] B. Abbott *et al.*, DØ Collaboration, Transverse Momentum Distributions of W and Z Bosons Produced in $\bar{p}p$ Collisions at $\sqrt{s} = 1.8$ TeV, Paper #464, Submitted to the *XXIX International Conference on High Energy Physics - ICHEP98*, July 23-29, 1998, Vancouver, B.C., Canada; B. Abbott *et al.*, DØ Collaboration, Phys. Rev. Lett. **80** 5498 (1998).
- [30] G. A. Ladinsky and C.-P. Yuan, Phys. Rev. **D50**, 4239 (1994). C. Balaczs and C.-P. Yuan, Phys. Rev. **D56**, 5558(1997); P. B. Arnold and R. Kauffman, Nucl. Phys. **B349**, 381 (1991).
- [31] F. Abe et al., CDF Collaboration, Phys. Rev. Lett. **79**, 4760 (1997); Phys. Rev. Lett. **79**, 2198 (1997).

- [32] R. Ansari *et al.*, UA2 Collaboration, Phys. Lett. **B215**:175,1988.
- [33] S. Abachi *et al.*, DØ Collaboration, Phys. Rev. Letters, **75**, 3226 (1995).
- [34] F. Abe *et al.*, CDF Collaboration, Phys. Rev. Lett. **81**, 1367 (1998).
- [35] F. Abe *et al.*, CDF Collaboration, Phys. Rev. Lett. **74**, 2626 (1995); S. Abachi *et al.*, Phys Rev. Letters **74**, 2632 (1995).
- [36] J. Alitti *et al.*, UA2 Collaboration, Z. Phys. **C49** 17 (1991).
- [37] T. Dorigo, CDF Collaboration, “ Observation of Z decays to b Quark Pairs at the Tevatron Collider”, *XXIX International Conference on High Energy Physics - ICHEP98*, July 23-29, 1998, Vancouver, B.C., Canada, hep-ex/9806022
- [38] B. Abbott *et al.*, DØ Collaboration “ Search for New Particles Decaying into Two-Jets with the DØ Detector”, Paper submitted to the *XVIII International Symposium on Lepton Photon Interactions*, July 28 - August 1, Hamburg, Germany.
- [39] J. Alitti *et al.*, UA2 Collaboration, Nucl. Phys. **B400**, 3 (1993).
- [40] F. Abe *et al.*, CDF Collaboration, Fermilab-Pub-97/023-E; FERMILAB-PUB-97/023-E. Submitted to Physical Review D Rapid Communications 1997; Phys. Rev. Lett. **74**, 3538 (1995).
- [41] S. Abachi *et al.*, DØ Collaboration, Phys. Lett. **B358** 405 (1995); Phys. Rev. Lett. **76** 3271 (1996); Phys. Lett. **B 385**, 471 (1996).
- [42] F. Abe *et al.*, CDF Collaboration, Phys. Rev. Lett. **79**, 2191 (1997)
- [43] B. Abbott *et al.*, DØ Collaboration, Search for High Mass Photon Pairs in $p\bar{p} \rightarrow \gamma\gamma jj$ Events at $\sqrt{s} = 1.8$ TeV, Submitted to the *XXIX International Conference on High Energy Physics - ICHEP98*, July 23-29, 1998, Vancouver, B.C., Canada
- [44] F. Abe *et al.*, CDF Collaboration, FERMILAB-PUB-98/252-E submitted to Phys. Rev.Lett.; Phys. Rev. Lett. **79**, 3819 (1997).
- [45] S. Abachi *et al.*, DØ Collaboration, Phys. Rev. Lett. **79**, 1197 (1997); B.Abbott *et al.*, DØ Collaboration, Phys. Rev. **D58**, 052001 (1998).
- [46] F. Abe *et al.*, CDF Collaboration, Phys. Rev. Lett. **80**, 5720 (1998).
- [47] B. Abbott *et al.*, DØ Collaboration, Phys. Rev. Lett. **80** 2063 (1998); B.Abbott *et al.*, Submitted to Phys. Rev. D , Fermilab-Pub-98/261-E.
- [48] F. Abe *et al.*, The CDF Collaboration, FERMILAB-PUB-98/319-E, hep-ex/9810029, submitted to Phys. Rev. Lett.; Phys. Rev. Lett. **80**, 2779 (1998).
- [49] F. Abe *et al.*, CDF Collaboration, Phys. Rev. Lett. **79**, 1992 (1997).

- [50] S. Kuhlman in D. Amidei & R. Brock, Ed. *Future ElectroWeak Physics at the Fermilab Tevatron: Report of the tev-2000 Study Group*, D. Amidei & R. Brock, Ed. Fermilab-Pub-96-082.
- [51] S. Kim, S. Kuhlman, W.-M. Yao, in *New Directions for High Energy Physics, Snowmass 96*, P 610, Ed. D. Cassel, L. Trindle Gennari & R.H. Siemann, July 1996; D. Hedin *ibid* P.608.
- [52] S. Kuhlmann, S. Bettelli, A. Bocci, D. Costanzo, R. Paoletti, S. Lami, ATLAS-PHYS-NO-106.
- [53] Fermilab SUSY/Higgs Run II Workshop-Higgs Working Group;
<http://fnth37.fnal.gov/higgs.html>.